The Abdus Salam
International Centre for Theoretical Physics

United Nations
Educational, Scientific and
Cultural Organization

IAEA
International Atomic Energy Agency

2167-22

Advanced School on Direct and Inverse Problems of Seismology

27 September - 8 October, 2010

Evidences on interactions between aseismic and seismic deformation processes

F.H. Cornet
Institut du Physique du Globe de Strasbourg
France

Evidences on interactions between aseismic and seismic deformation processes

François Henri Cornet
Institut de Physique du Globe de Strasbourg

Evidences from large scale in situ experiments

- Indirect evidence from stress measurements : example at Le Mayet de Montagne
- Direct evidence at the Soultz sous forêts European experimental geothermal site

Evidences of natural aseismic motion occurrences : The Corinth Rift Laboratory

Results from the Le Mayet de Montagne Geothermal Laboratory

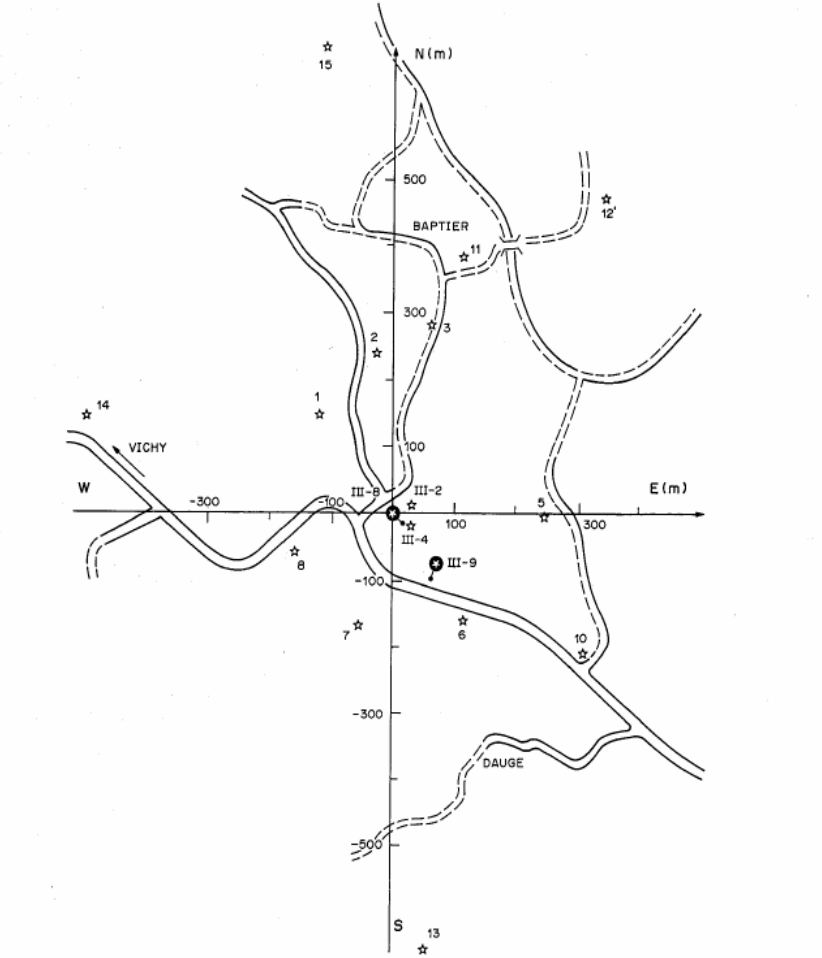

Fig. 1. Location of seismic stations (☆) and of boreholes used for the hydraulic injections (✪). Scale is in m.

- An in situ 800 m deep laboratory on fluid percolation in fractured rock masses (granite) has been developed in the eighties, under French and European funding, for investigating the possibility of exploiting heat from deep hot rock formations.
- The main objective was to test the possibility of stimulating a granitic rock mass in order to develop an efficient heat exchanger out of the natural fracture network.
- The ideas was to build up progressively pore pressure so as to induce shear along optimally oriented fractures. This required preliminary understanding of both the regional stress field and the natural fracture system. Monitoring of induced seismicity was conducted for all stimulation experiments with a 14 3C-station network.

Observed microseismic activity

- The 1985 stimulation (about 2200 m^3)

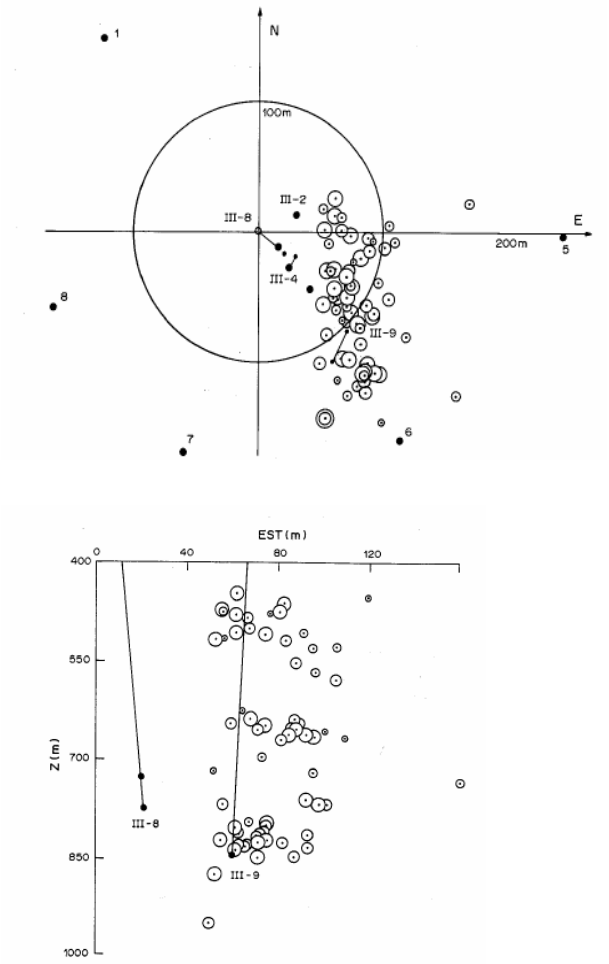

The 1986 stimulation (over 42 800 m^3)

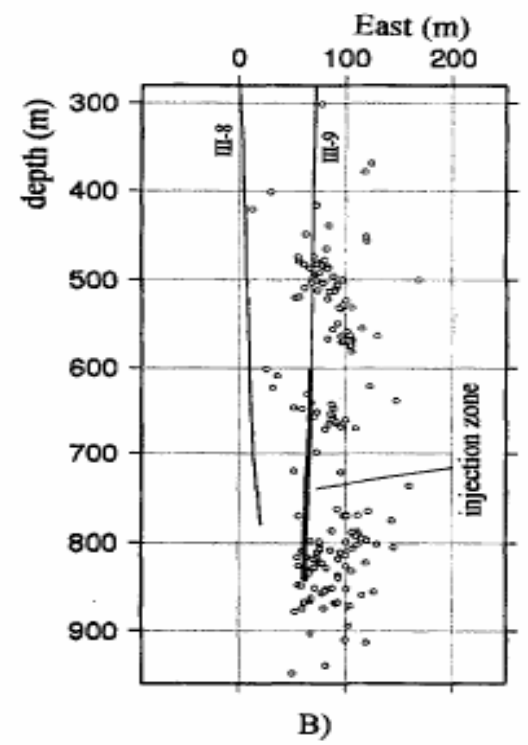

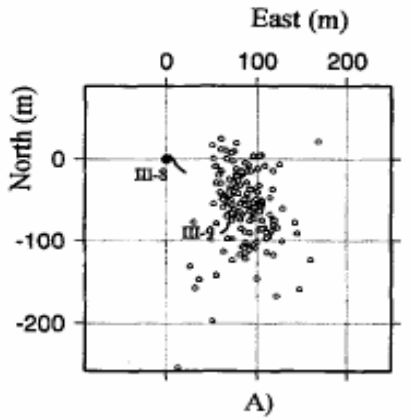

Independent stress determinations from hydraulic tests and from focal mechanisms inversions

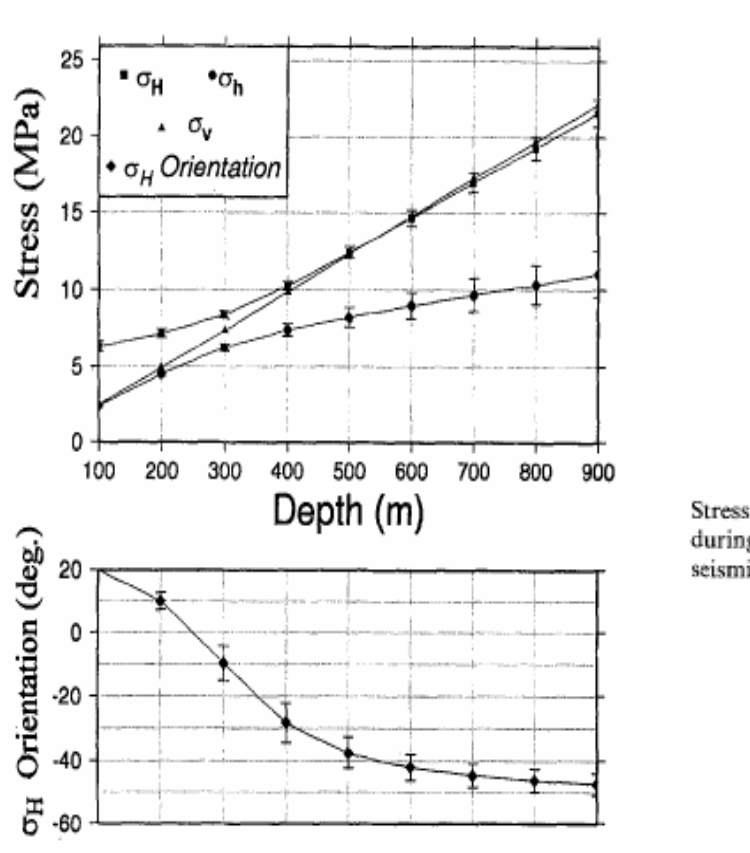

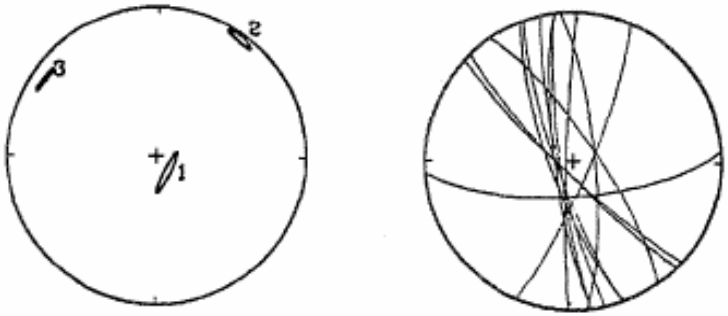

Figure 3
Stress determination derived from the inversion of focal mechanisms of the microseismic events observed during the preliminary reservoir development (total injected volume of 2200 m^3). Only the deepest seismic domain (see Fig. 1B) is considered. The stereographic projection of the principal directions is shown on the left. The orientation of selected planes is shown on the right.

Results from joint inversion of hydraulic tests and focal mechanisms (Cornet and Yin, pageoph, 1995)

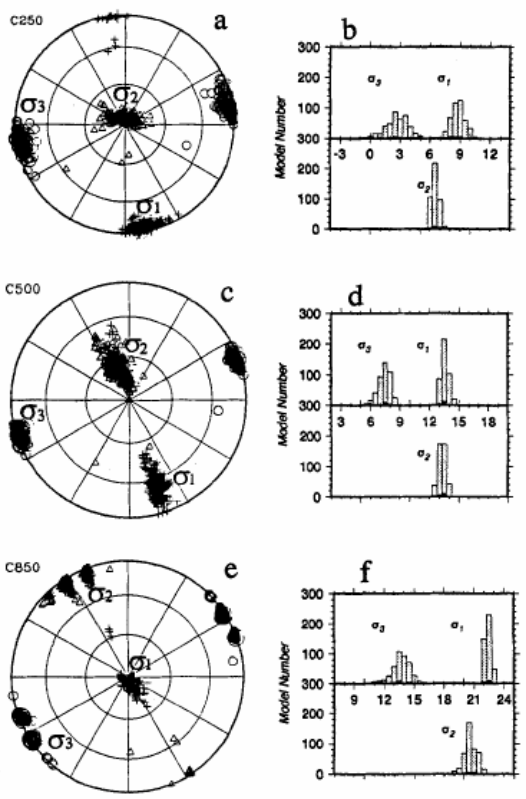

Figure 5
Stress determination obtained after integrating 22 HTPF measurements and 87 focal mechanisms. The stress field is presumed to vary linearly with depth. Results are shown at three different depths (250 m, 500 m, 850 m). a), c) and e) refer to the principal stress directions while the magnitudes (in MPa) are shown on b) d) and f). These results correspond to 430 models which are included within 95% confidence level.

- Results from the joint inversion is compatible with more than 90 % of hydraulic data but only 70 % of focal mechanisms.
- It is proposed that 30% of focal mechanisms are associated with zones of heterogeneity (size of events ranges from 1 to 10m)

Hydraulic tests for stress measurements conducted after the long term circulation experiment confirm zones of heterogeneity consistent with aseismic slip

(Scotti and cornet, Int J Rock Mech Min Sc., 1994)

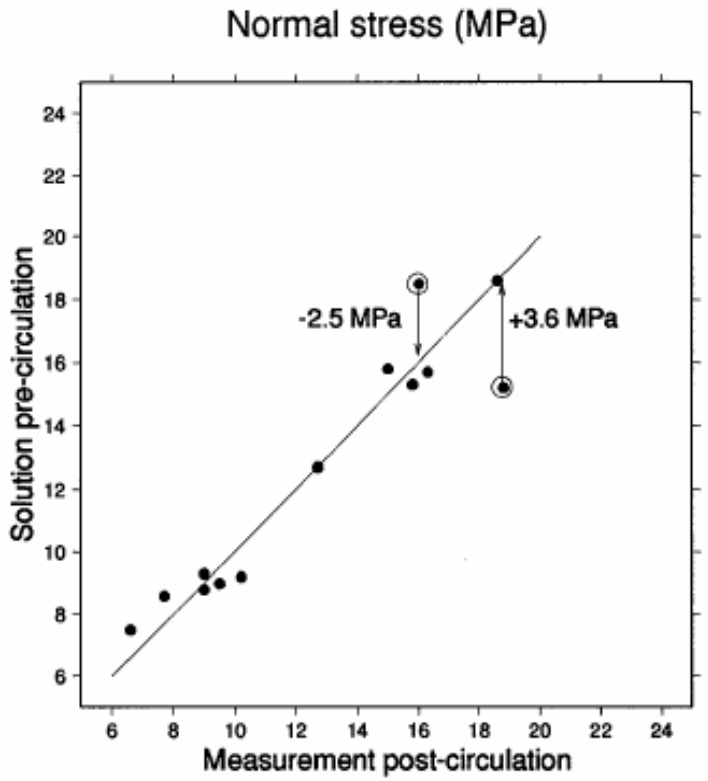

Fig. 2. By comparing the 13 post-circulation measurements to the pre-circulation solution it was possible to identify two extremely heterogeneous HTPF measurements. Notice that one perturbation is positive and the other is negative. Exact values are given in Table 1.

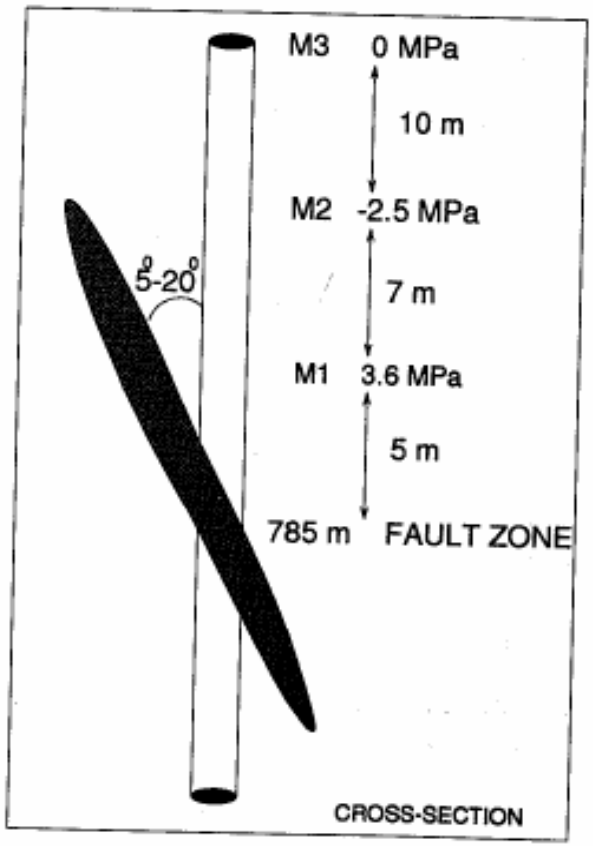

Fig. 5. Cross-sectional view of the modeled fault geometry at 785 m depth in the INAG III-9 well.

Conclusion from Le Mayet de Montagne

- Inversion of focal mechanisms alone for principal stress direction determination may not be accurate because of local stress heterogeneity.

- One of the causes for the source of heterogeneity is aseismlic slip induced by the fluid injection.

Some results from the Soultz-sous-forêts European experimental site

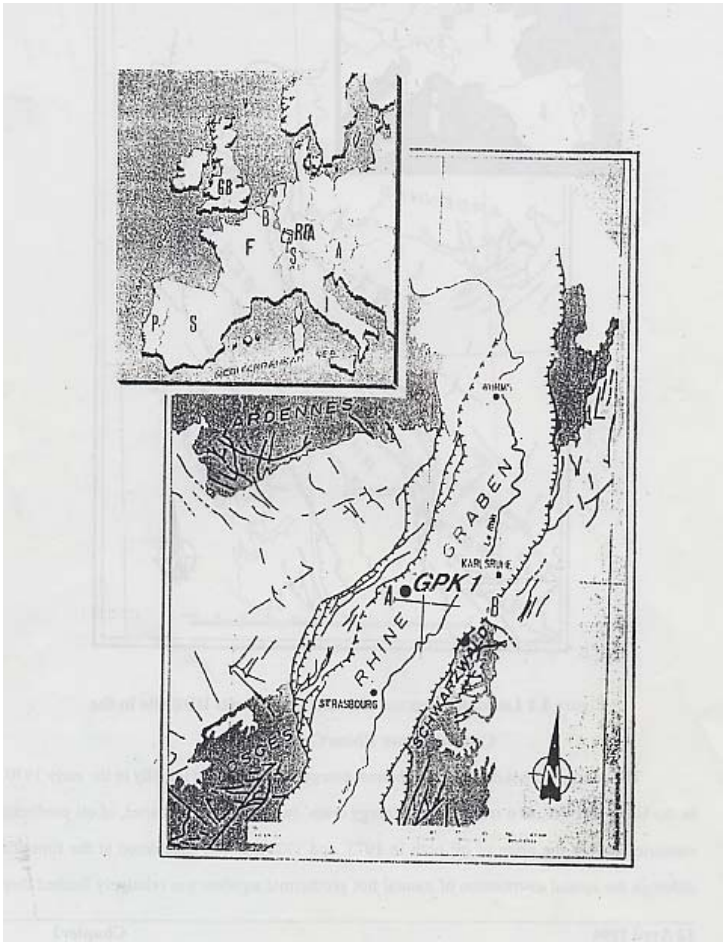

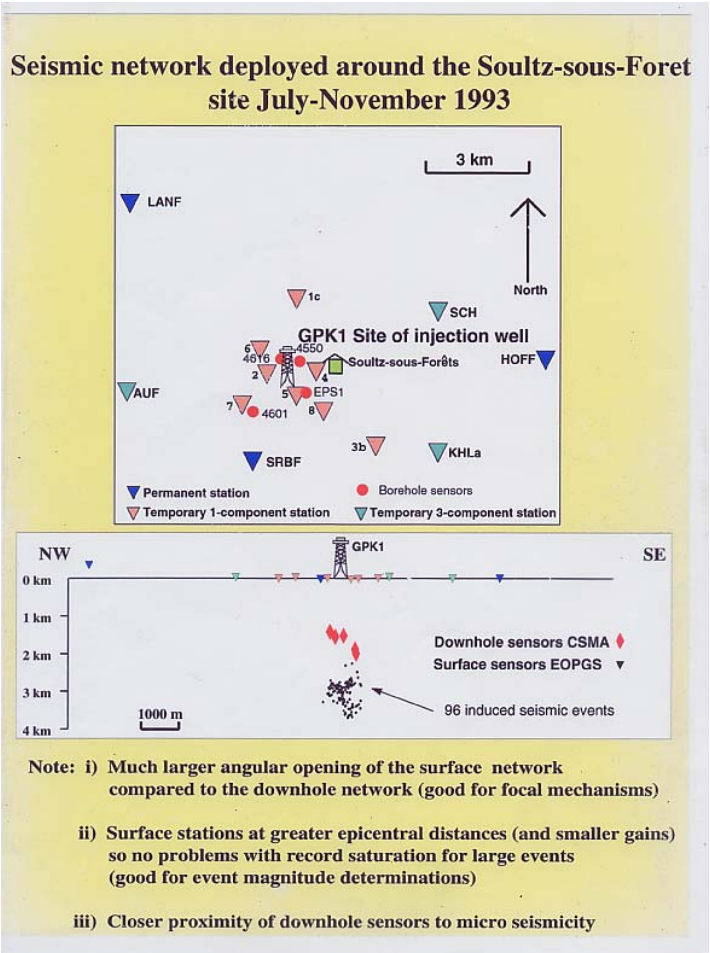

Compression breakouts observed in well GPK1 around 3440 m

Cornet, Berard and Bourouis, IJRMMSc 2007

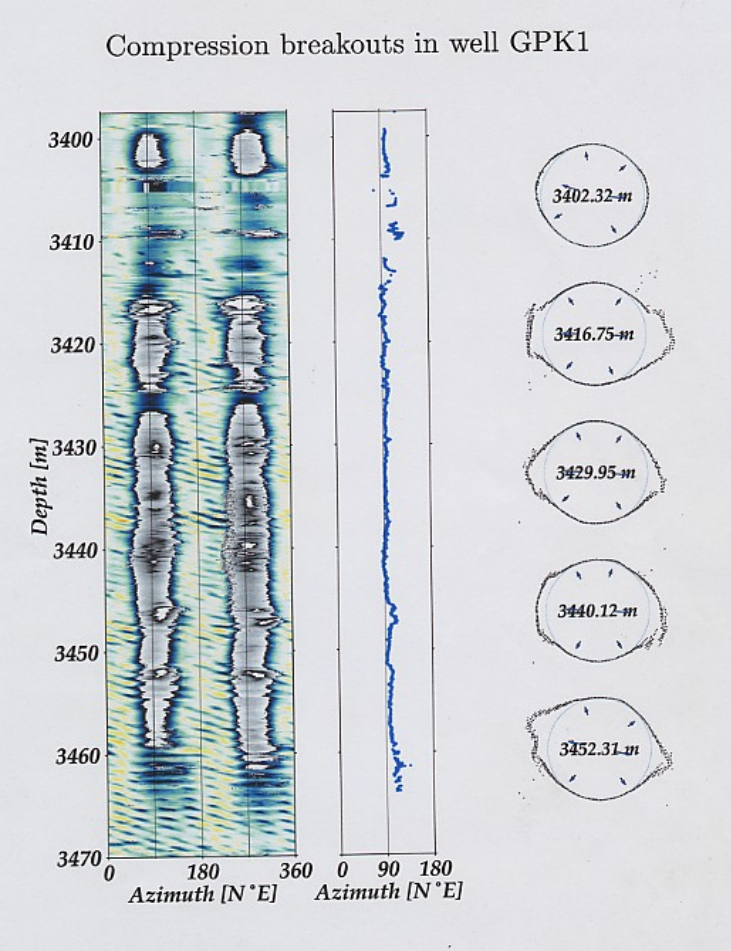

- Compression breakouts are indicative of zones of highest tangential compressive stress :

  $-\sigma_h + 3\,\sigma_H - P_b - f(P_0) - \alpha E \Delta\theta / (1-\nu) = \sigma^c$

- No breakouts seen initially in GPK1, No breakouts in GPK2 just after drilling, some seen sometime after drilling : problem of time dependency for breakout development.

- Recall loading rate effect on rock strength (e.g. Hudson & Brown, 1973)

Results from large scale hydraulic reconnaissance test (2850-3400 m) (Sept. 1993)

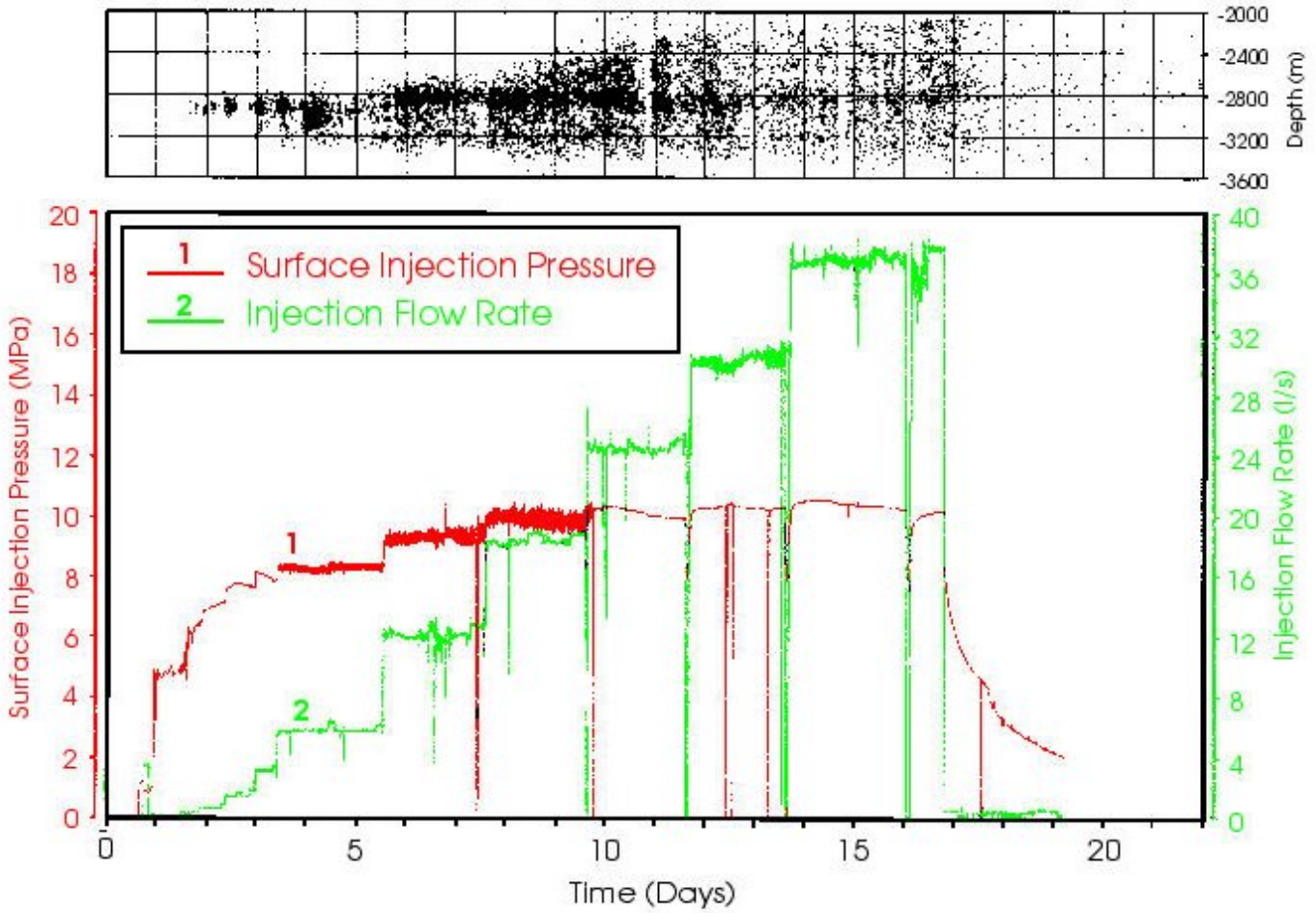

Location of induced microseismic events

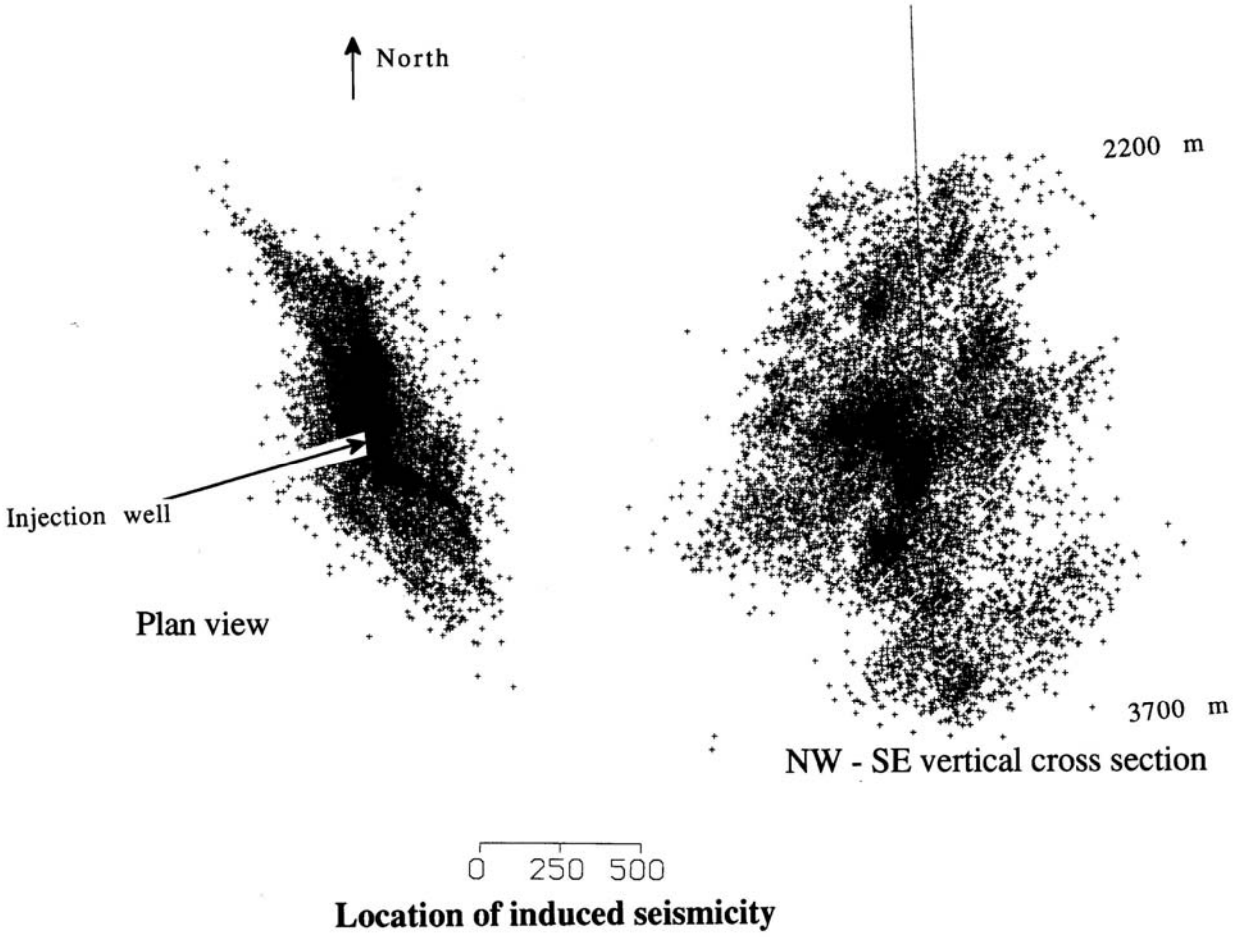

Location of induced seismicity

Closer analysis of horizontal direction of microseismic cloud

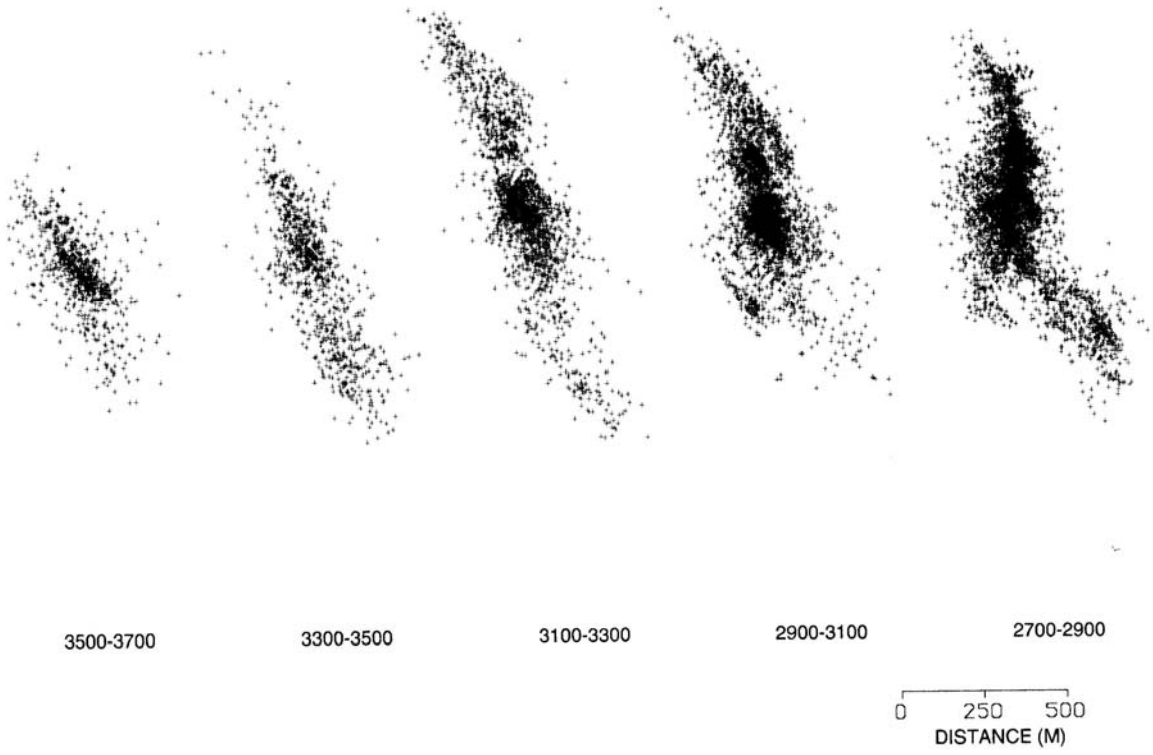

Analysis of fault plane solutions from induced microseismicity

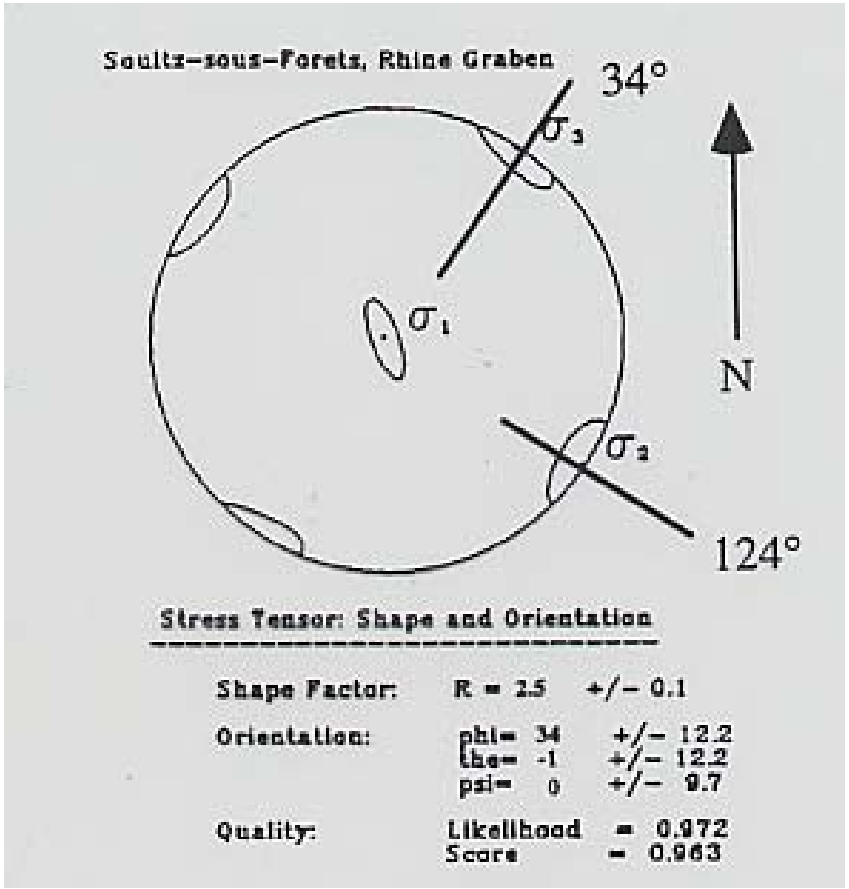

- 2 nodal planes for each focal mechanism
- Slip vector **S** in nodal plane is parallel to resolved shear stress τ in nodal plane

  S . τ / | τ | = 1

  τ = Tn – (Tn.n)n

$$(\sigma) = \sigma_1(1) + (\sigma_3 - \sigma_1)\begin{pmatrix} 0 & & \\ & 1 & \\ & & R \end{pmatrix};$$

$$R = (\sigma_2 - \sigma_1)/(\sigma_3 - \sigma_1)$$

Heterogenity in stress direction

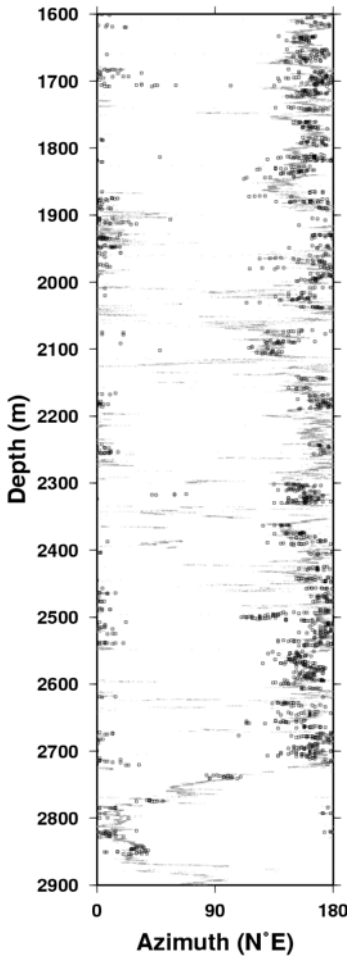

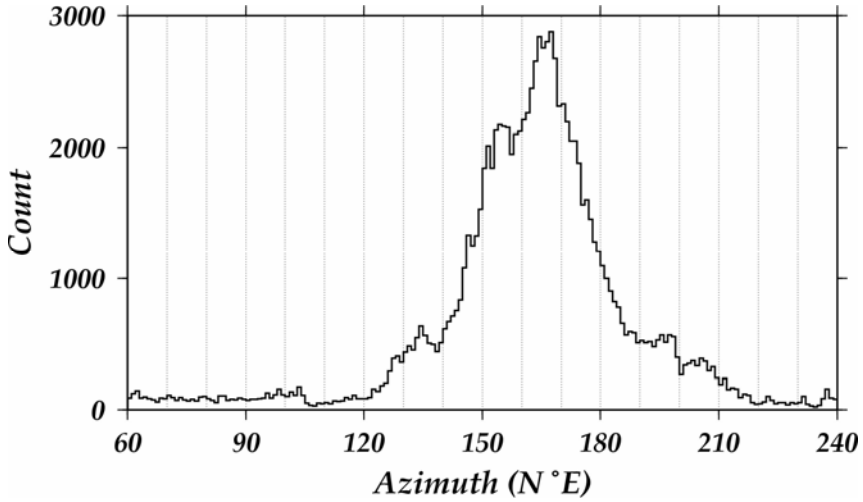

Focal mechanisms and stress directions

- Stress perturbation caused by previous events

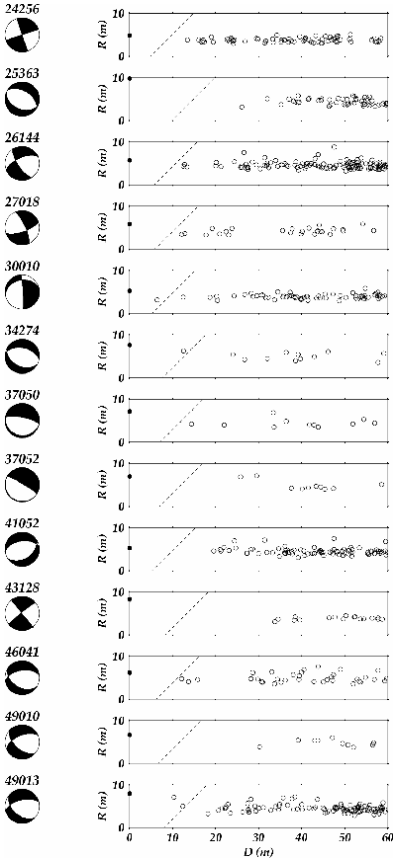

- Characterization of preexisting stress heterogeneity

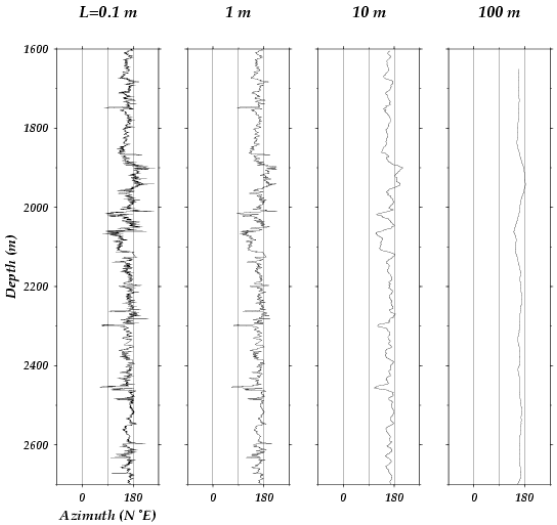

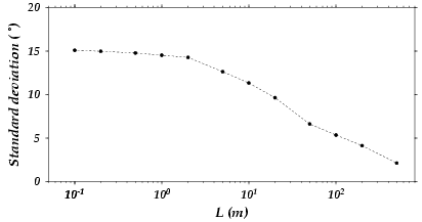

Principal stress direction determination from shear wave splitting analysis

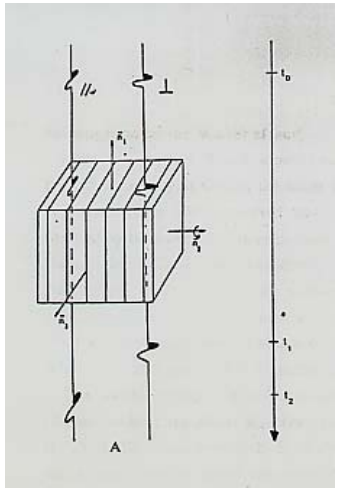

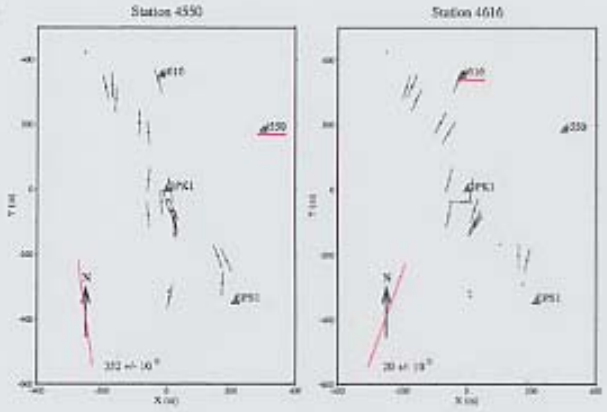

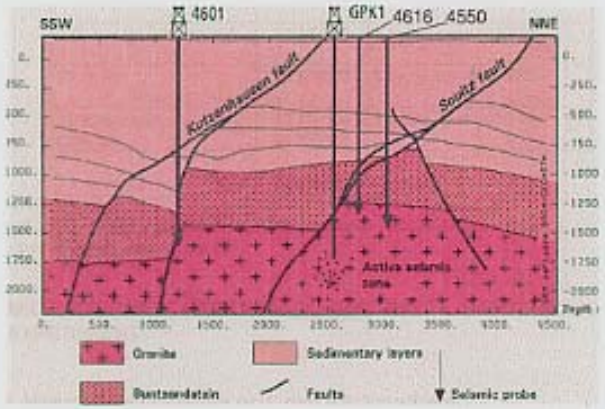

- S wave splitting

⇐ hexagonal anisotropy with a N-S horizontal symmetry axis, consistent with σ_H

- Stress rotation

⇐ topography of the sediment-granite boundary

Direct evidence of aseismic slip

(Cornet, Helm, Poitrenaud and Etchecopar, Pageoph, 1997)

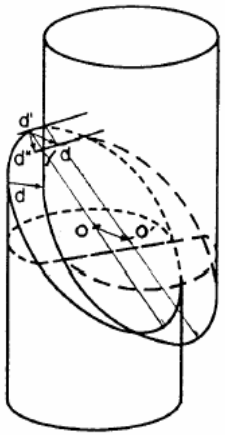

Existing fracture

Borehole geometry result from shear displacement along existing fracture (general case):

d = Displacement
d' = Strike component
d" = Dip component

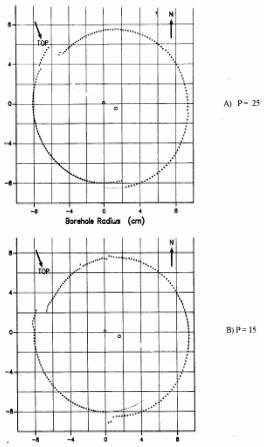

Determination of slip motions induced in the well GPK1 during the September–October 1993 injections. Z is distance from well head (in m) according to the logging depth meter, β is the dip direction of fracture plane (positive eastward), α is the dip of fracture plane, λ is the strike of the slip vector, A is amplitude of the slip motion (in cm). Uncertainties are noted ε with the respective subscript. SX is the mean amplitude of the slip vector measured within the cross section of the borehole. Frame of reference is north, east, vertical positive downward. Within the fracture plane, rotation is positive from strike direction toward dip (downward positive).

Z (m)	β	α	λ	A (cm)	ε_λ	ε_A (cm)	SX (cm)	ε_{SX} (cm)
2966	105	84	110	4.7	5	0.7	0.5	0.1
2867	259	62	304	2.2	3	0.1	1.45	0.07
2976	269	61	218	0.8	15	0.2	0.5	0.05
2887	298	75	271	0.85	8	0.3	0.28	0.1
2973	273	78	198	0.4	10	0.06	0.22	0.04
2925	48	86	99	4.3	13	1.3	0.5	0.14

Conclusion from Soultz sous forêts

- Stress field is presently well established down to 5 km. The maximum horizontal principal stress is oriented N170°E.

- Inversion of focal mechanisms of events with magnitude larger than 1.7 yields similar answers but do indicate existence of local heterogeneity.

- Ultrasonic Borehole Imager (UBI) identifies slip along preexisting planes; some of them reach 4 to 5 cm. These slips occurred in an aseismic manner.

Results from the Corinth Rift Laboratory

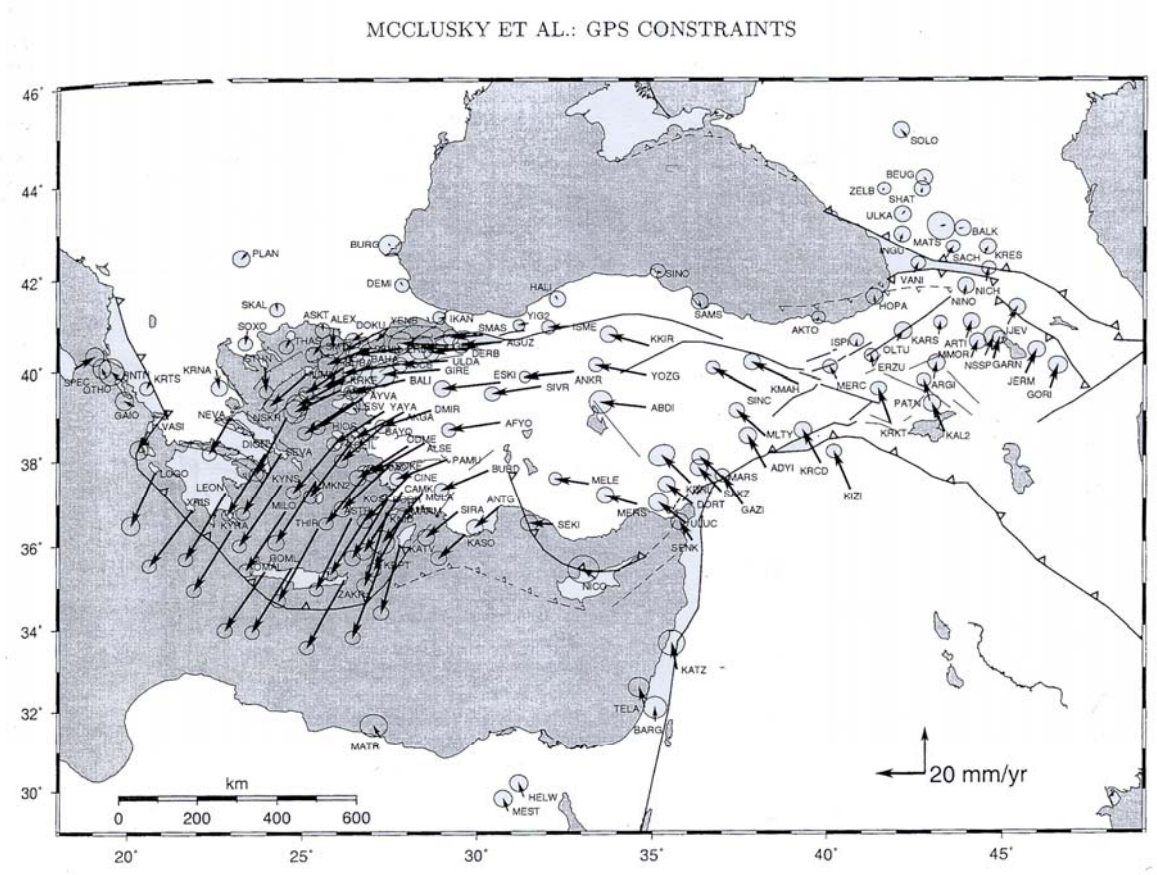

Figure 2. GPS horizontal velocities and their 95% confidence ellipses in a Eurasia-fixed reference frame for the period 1988–1997. To avoid clutter, we have omitted plotting some sites in the Marmara region, but in Table 1 we list velocities for all sites. Tectonic symbols are as in Plate 1.

Influence of roll back in the Aegean area

from L. Royden, 2007

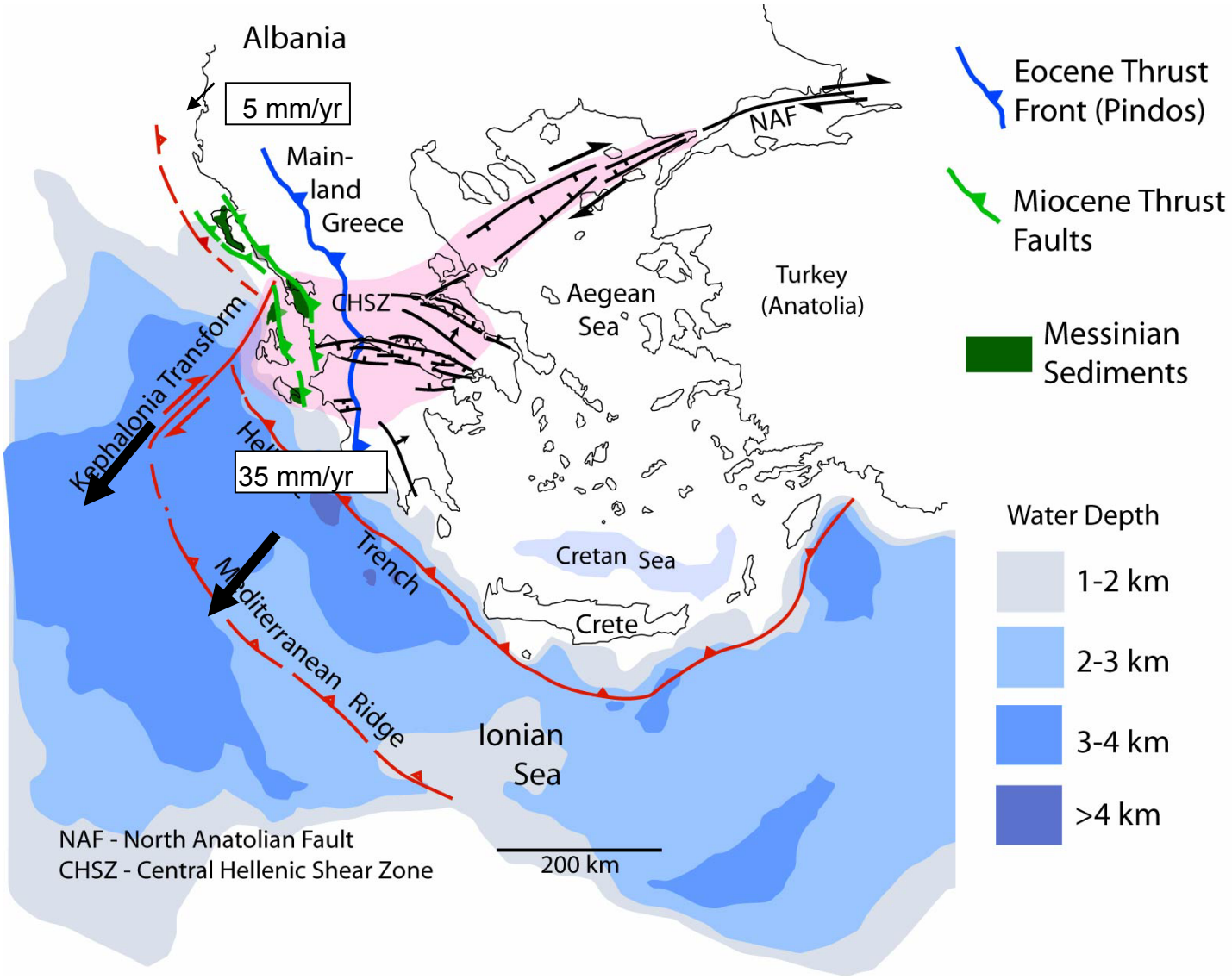

Seismic activity in Greece 1970-2007

from National Observatory of Athens Catalog (Bourouis & Cornet, GJI, 2009)

- Cumulated energy

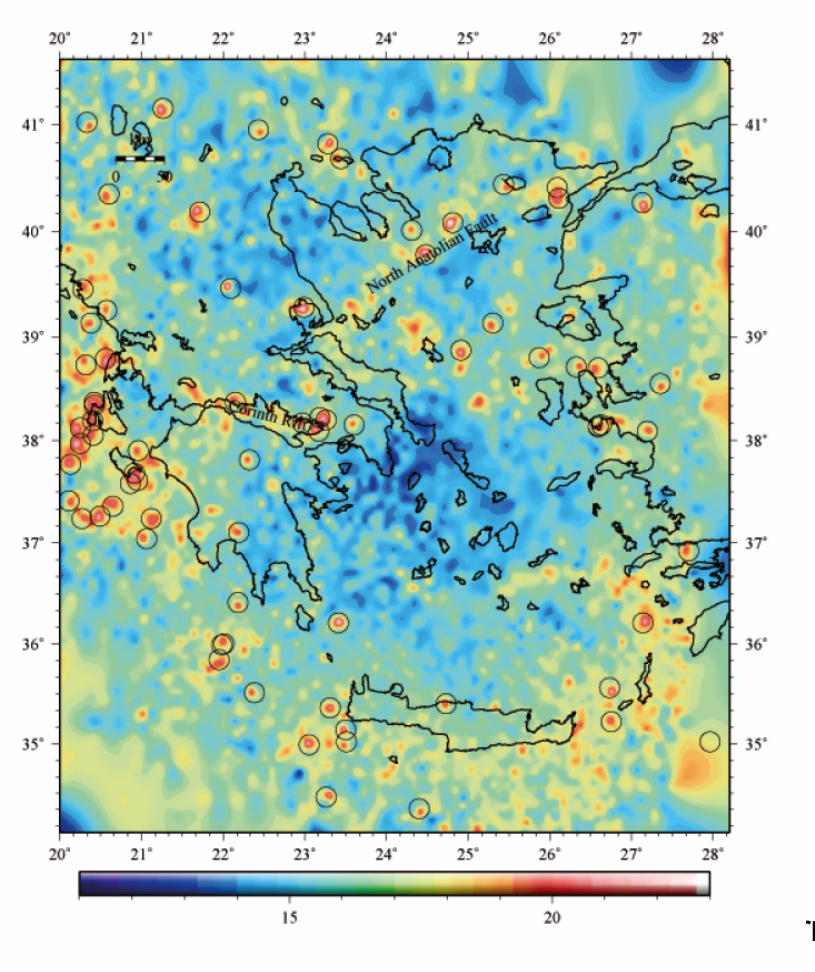

- Nb of events

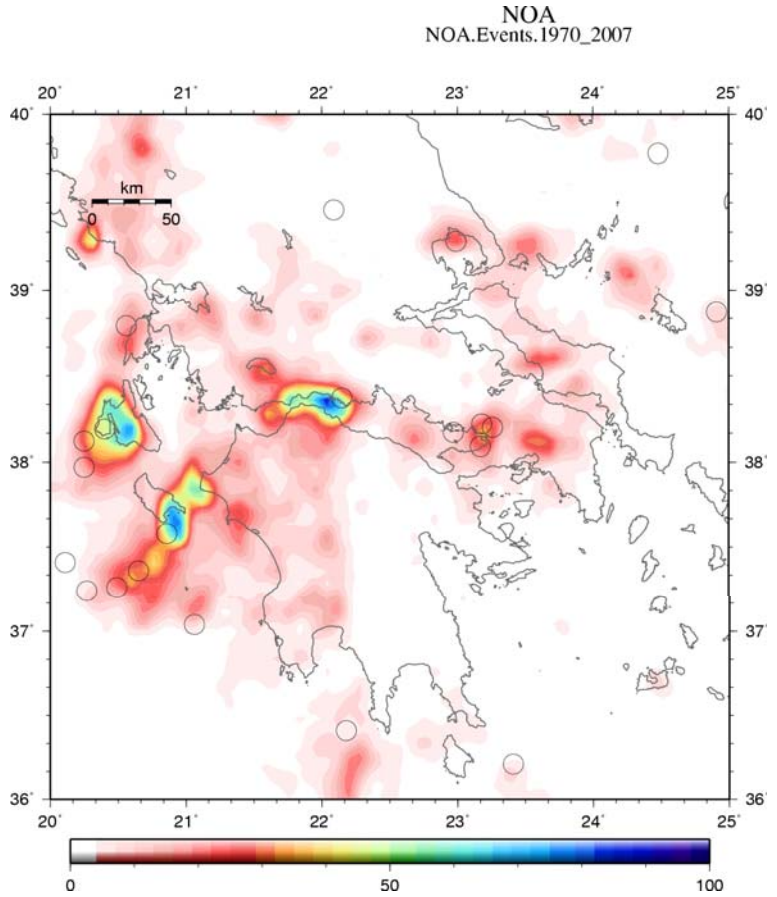

European seismicity

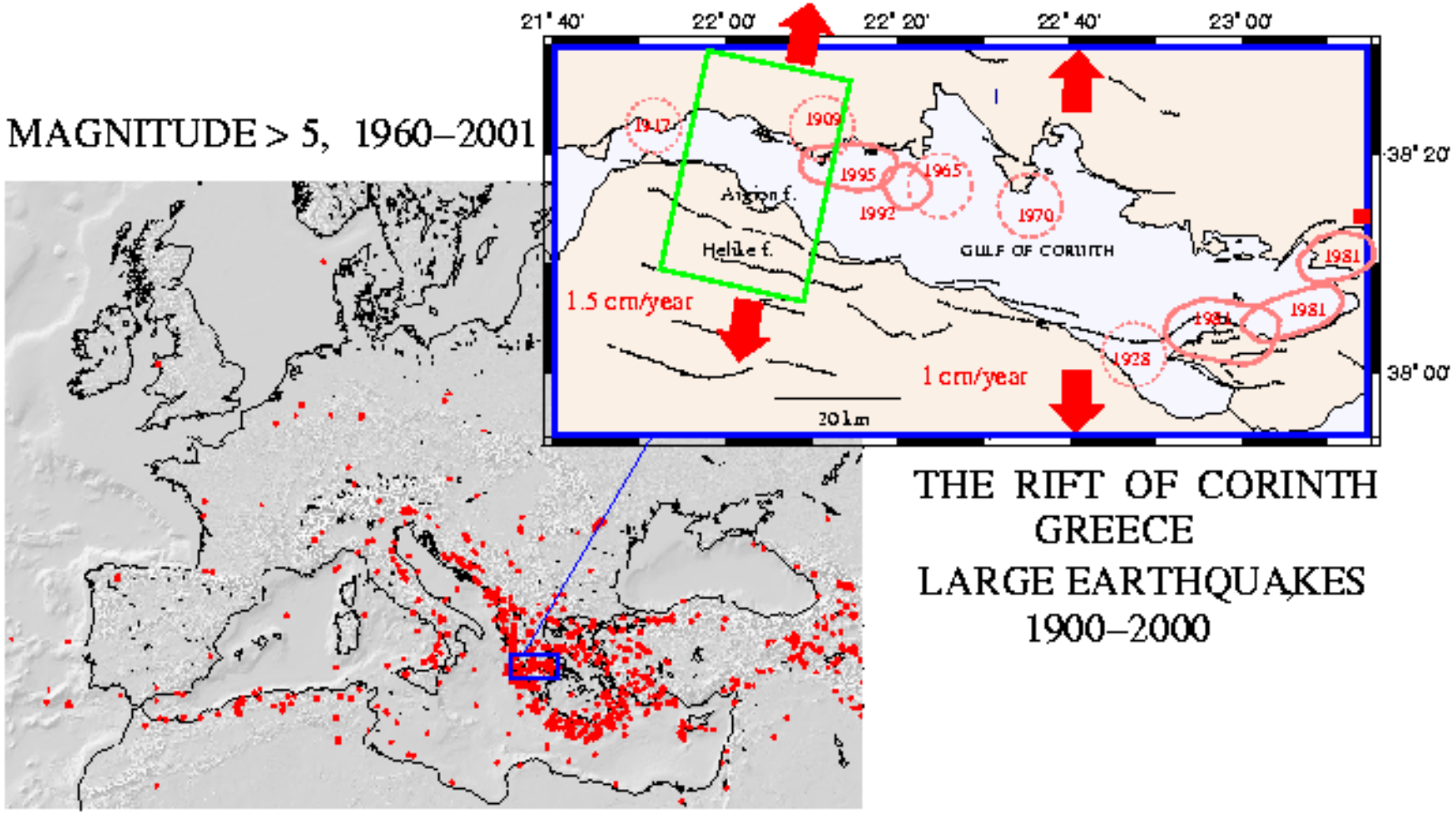

Geological background (Jolivet et al. 2004)

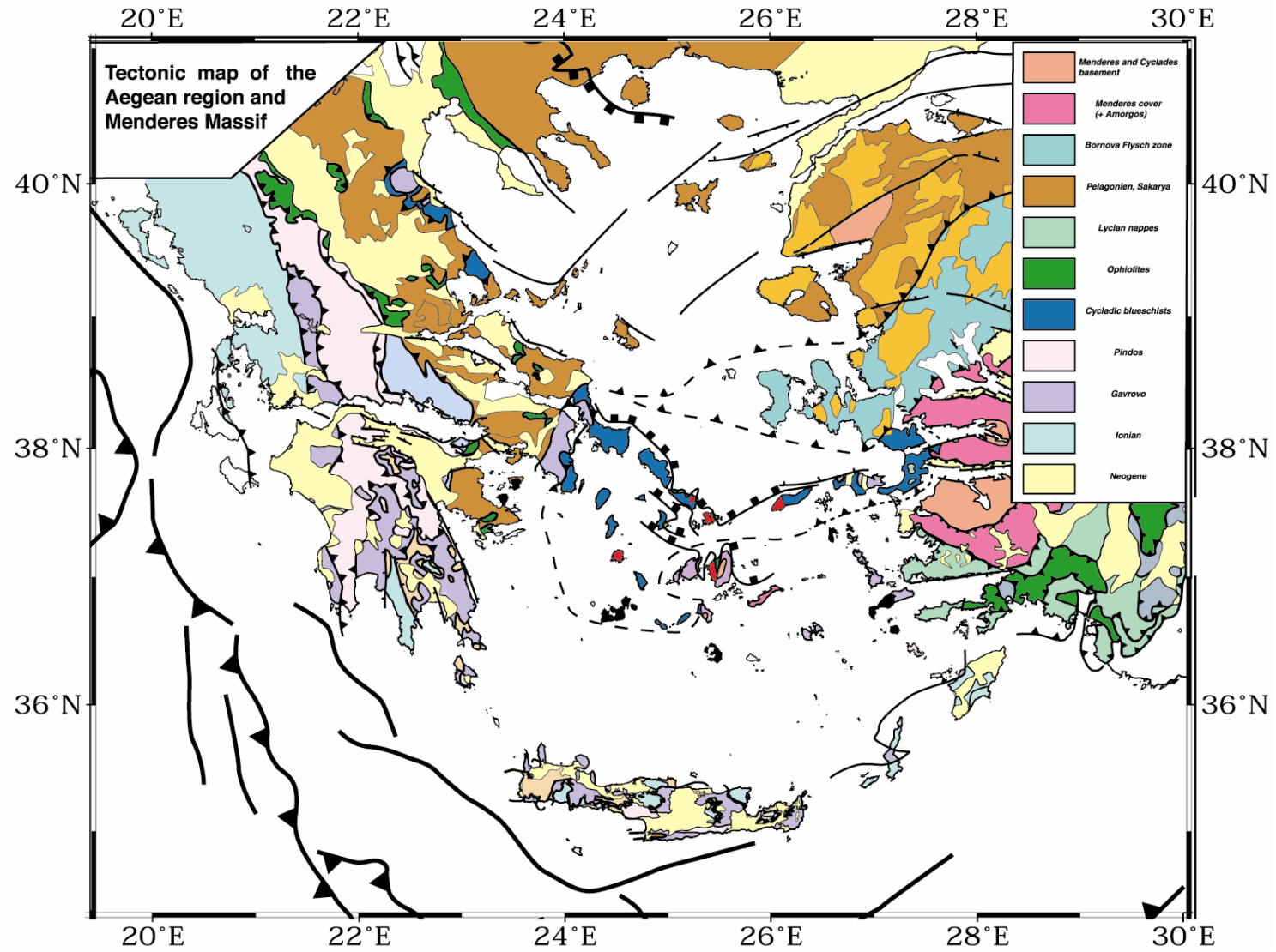

Structural cross section as defined in 1996

(Rigo et al., 1996, Lemeur et al. 1994)

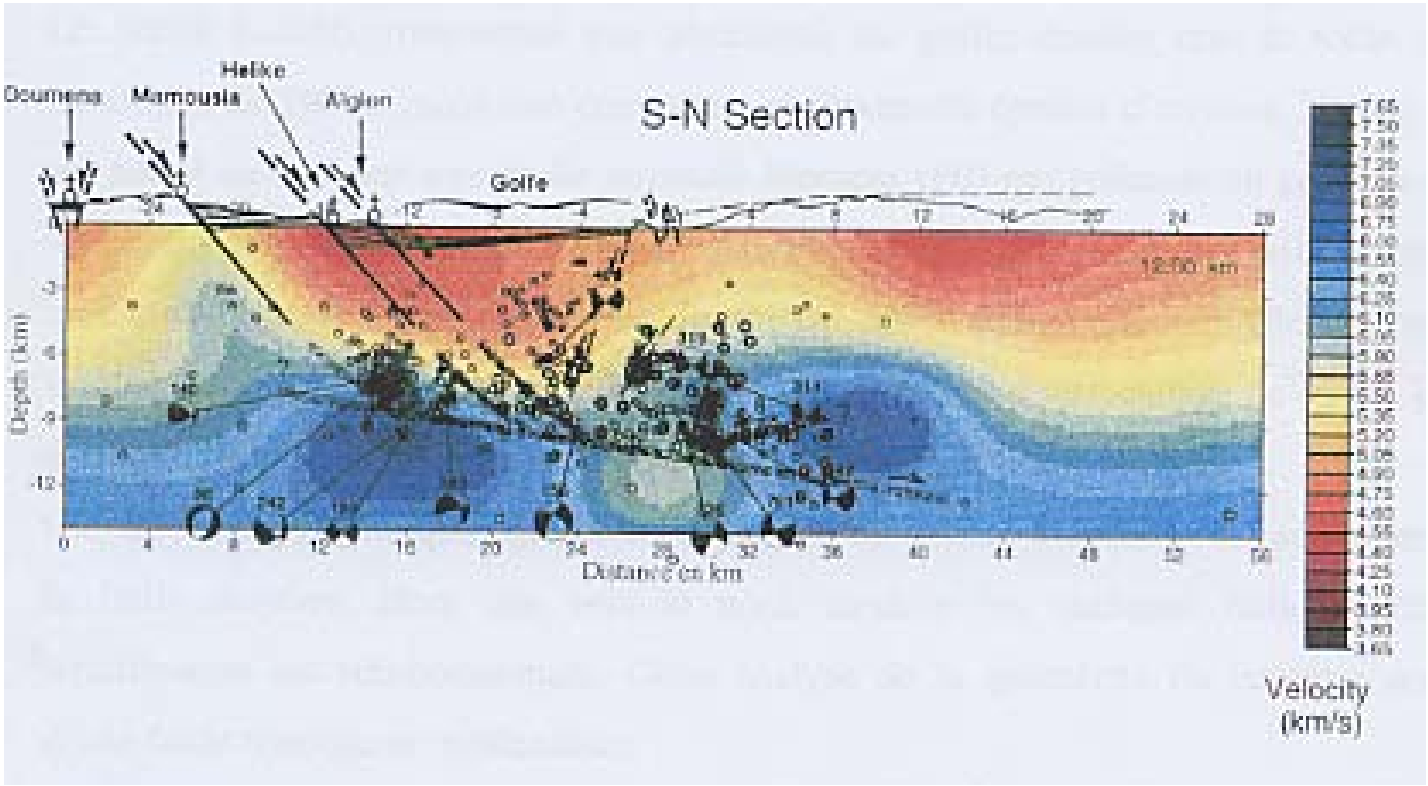

Simplified cross section for ICDP supported AIG10 well

(Cornet et al., Naville et al., Rettenmayer et al., CR-Geosciences, 2004)

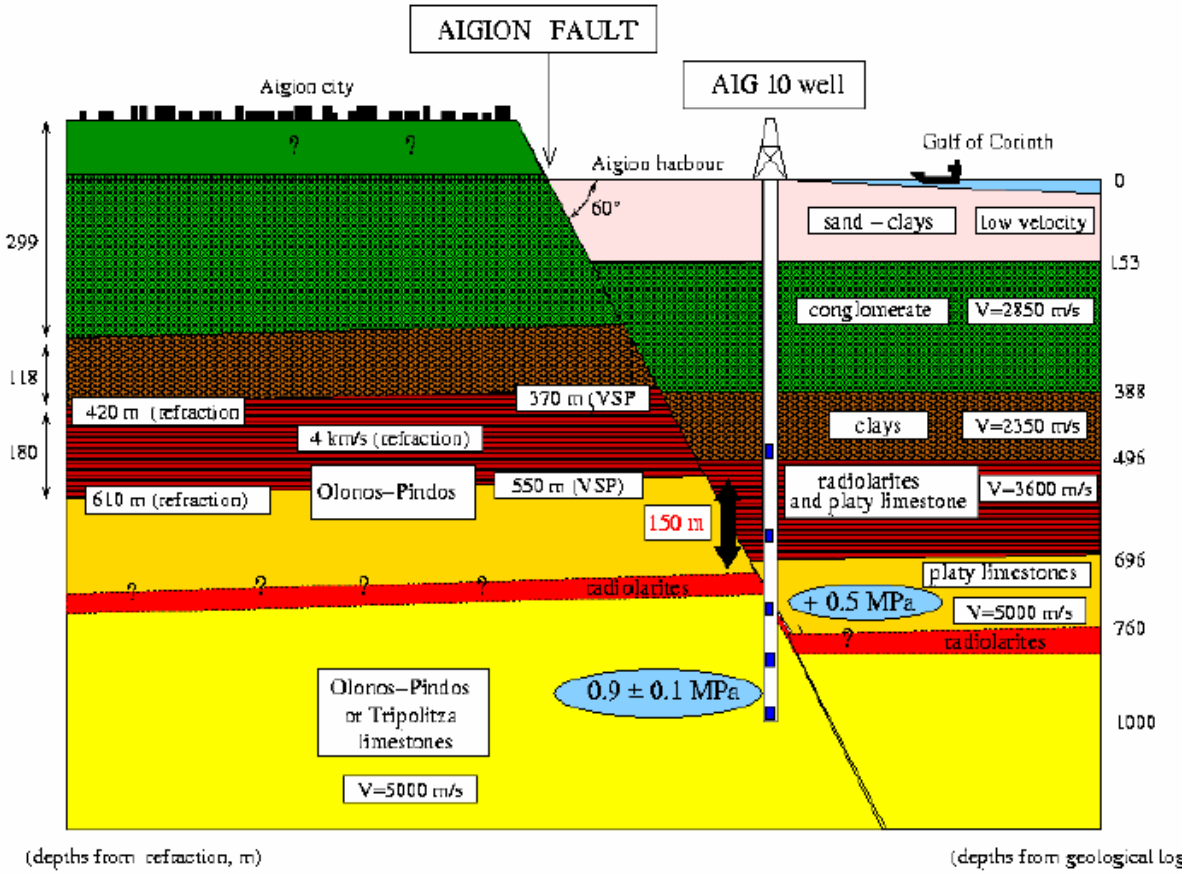

- Fault length : between 10 and 15 km
- Age of the fault of the order of 100 ky
- Mean fault velocity from 1.6 to 4.3 mm/y (according to paleosismology by trenching)

ICTP-Cornet-sept-2010

On the hydraulic properties of faults

from Nojima fault – Locker et al. (2000?)

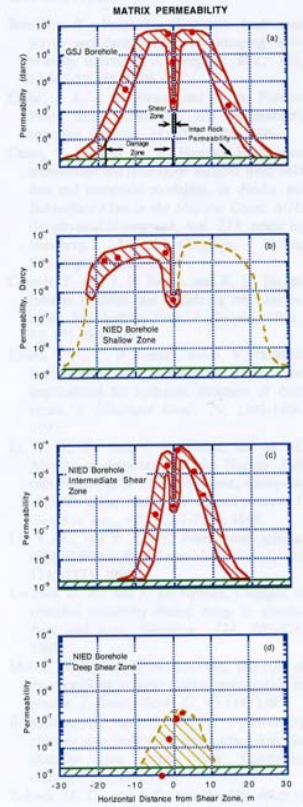

Figure 4. Profiles of matrix permeability measured at 50 MPa effective confining pressure. The three upper fault crossings show a low permeability shear zone axis surrounded by high permeability damage zones. The deep shear zone is partially sealed and was apparently not activated by the Kobe earthquake.

- Faults constitute hydraulic barrier perpendicularly to the fault direction but are hydraulically conductive parallel o the fault direction

Downhole Instrumentation deployed June 17 2007

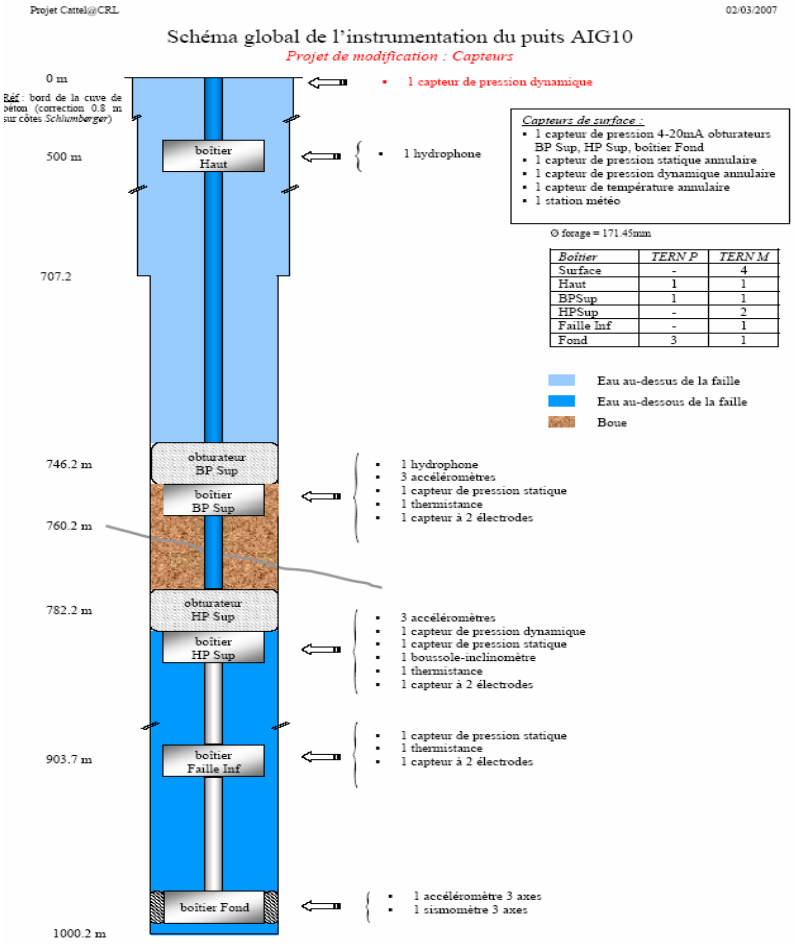

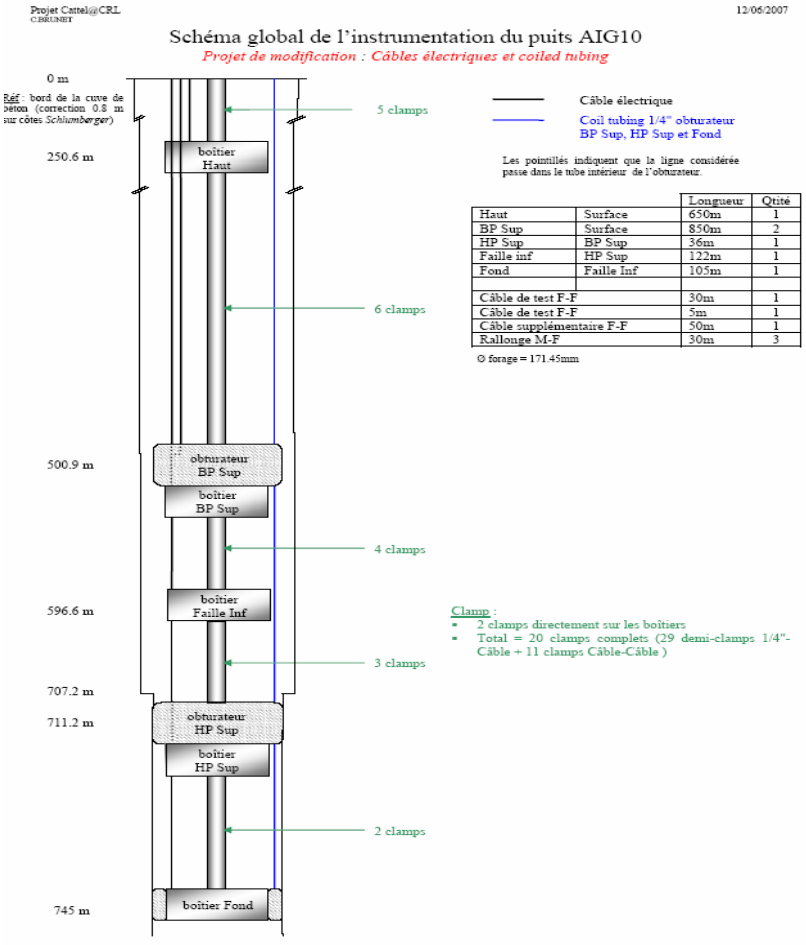

Temperature and water pressure in AIG10

(Doan et Cornet, EPSL, 2007a; GRL, 2007b)

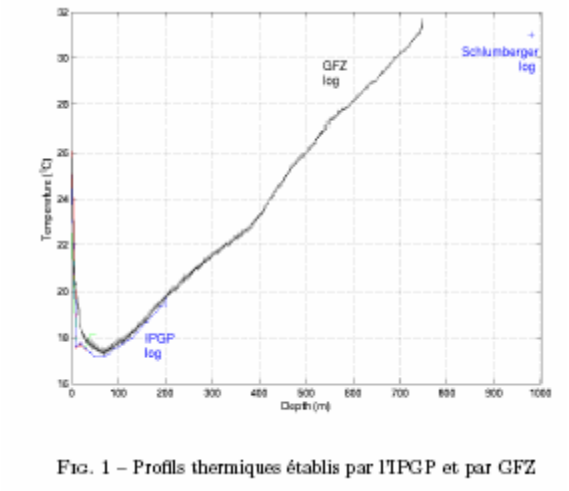

FIG. 1 – Profils thermiques établis par l'IPGP et par GFZ

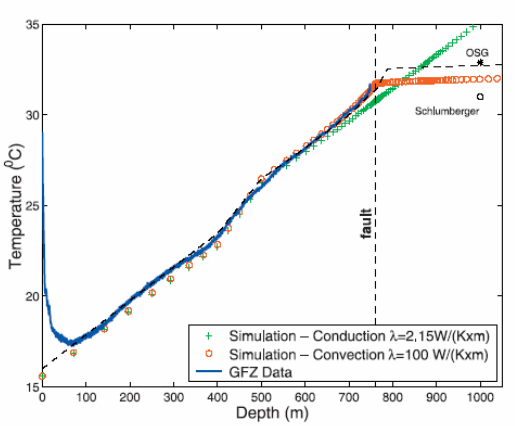

Figure 3. Comparison of thermal data obtained by GFZ (continuous blue line) and the thermal profile produced with the model of Figure 2. The profile obtained for a karst in convection (red circles) fits very well the actual data, in contrast with that computed for a karst in thermal conduction. The model can be refined by modeling the boundary layer at the boundary of the convection cell with an arbitrary 10 m thin layer along the boundary of the karst, with a conductivity of 0.9 W/(K × m). The resulting model (black dashed line) fits better the OSG data (black asterisk) while staying close to the curve computed with the simple convective case.

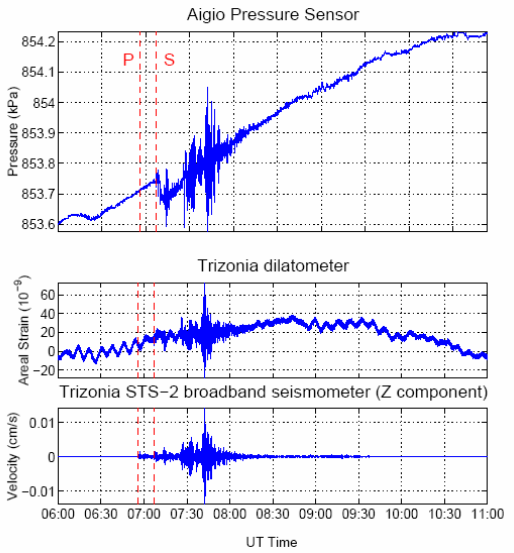

- Heat flow : 53 mw/m^2; convection in the karst
- Pressure gauge sensitivity : 10^{-4}μstrain
- Karst storativity : 7.7±2 10^{-7} m^{-1}
- Karst permeability :~ 10^{-12} m^2
- Upper and lower aquifers are confined

- Some teleseisms induce local effects

First results from the downhole pressure recording

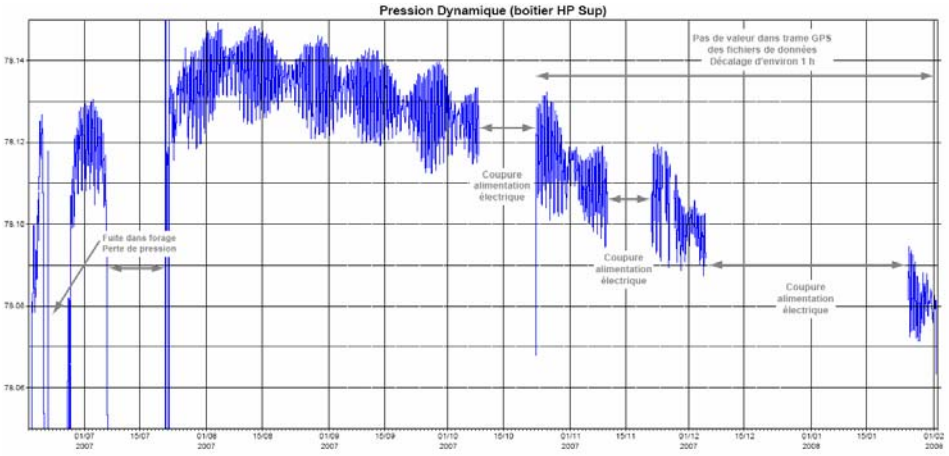

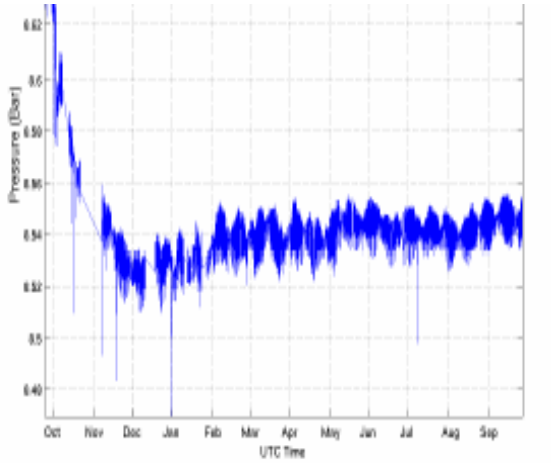

- Top : June 2007-Feb 2008,
  production flow rate 11 m^3/h
- Right : Oct. 2003-sept. 2004
  Production flow rate 250 m^3/h (sept. 2003)

Rift seismicity during the AIG10 well observation period (June – September) 2007

- (a) events detected with CRLNet alone (11 3C-stations, 2 HZ).
- (b) number of events per day.
- (c) Histogram of moment magnitudes (automatic evaluation).
- (d) Gutenberg-Richter distribution.

- This seismicity is used to calibrate the velocity model and the time synchronization between AIG10 stations and CRLnet.

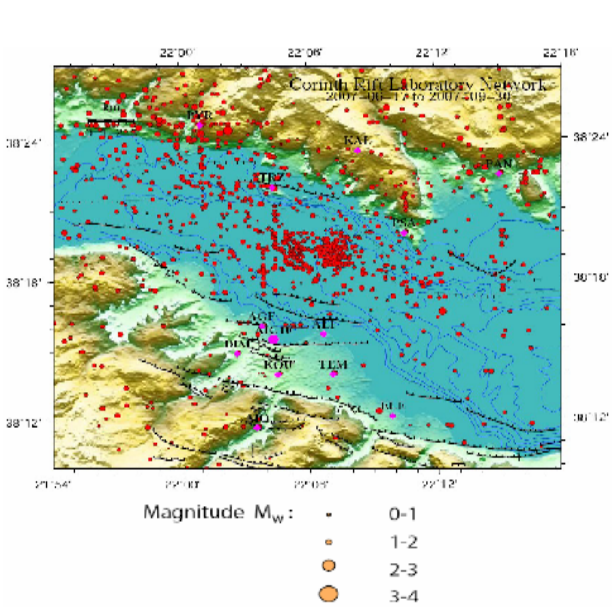

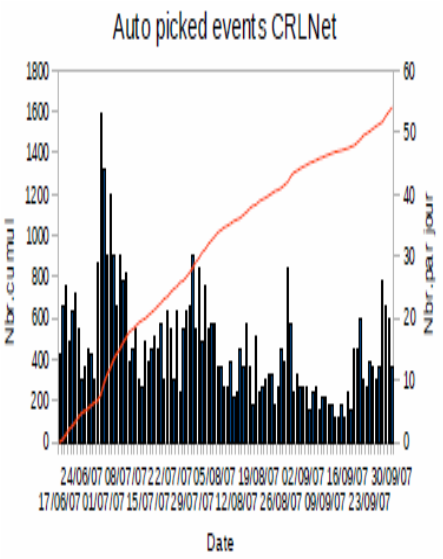

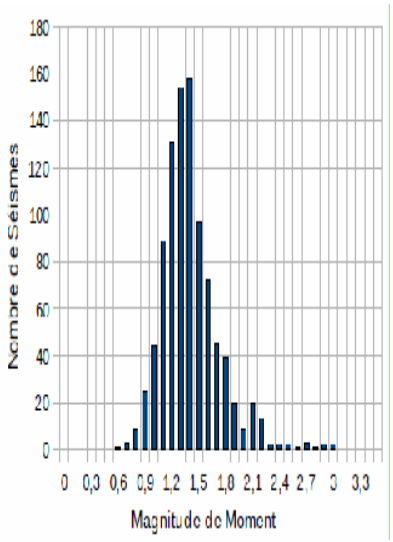

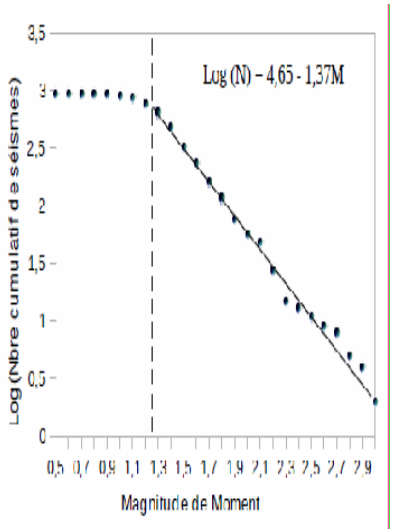

- Gutenberg-Richter distribution suggests that the catalogue is complete only for Mw > 1.4 (Fig. d).

- The high value for the b coefficient (b=1,37) suggests a heterogeneous zone in which deformation induces small events either because of pore pressure variations, creep through a large volume, or both.

Events identified with AIG10 sensors

Because one horizontal component is missing on geophone, location of events is made with the help of CRLNet stations.

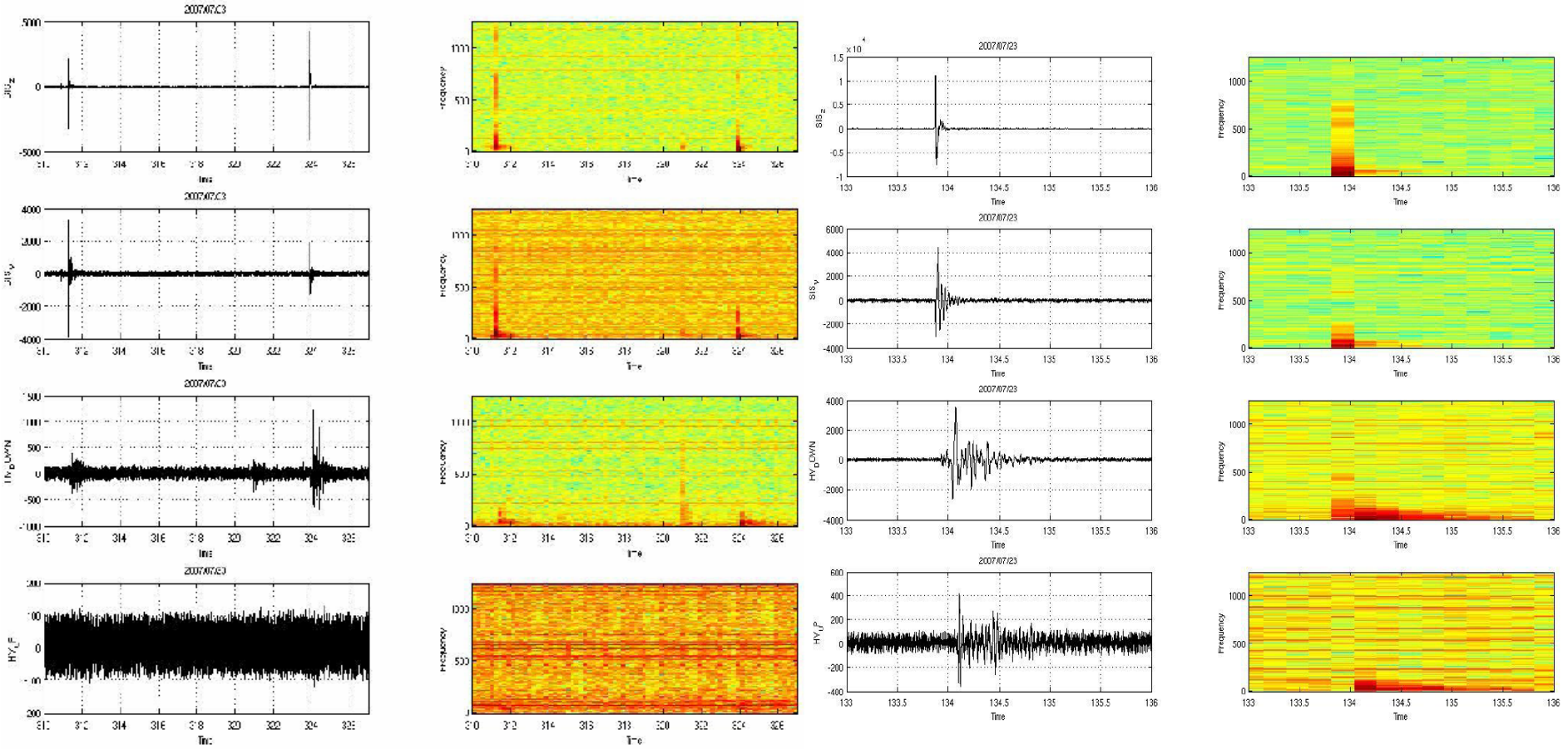

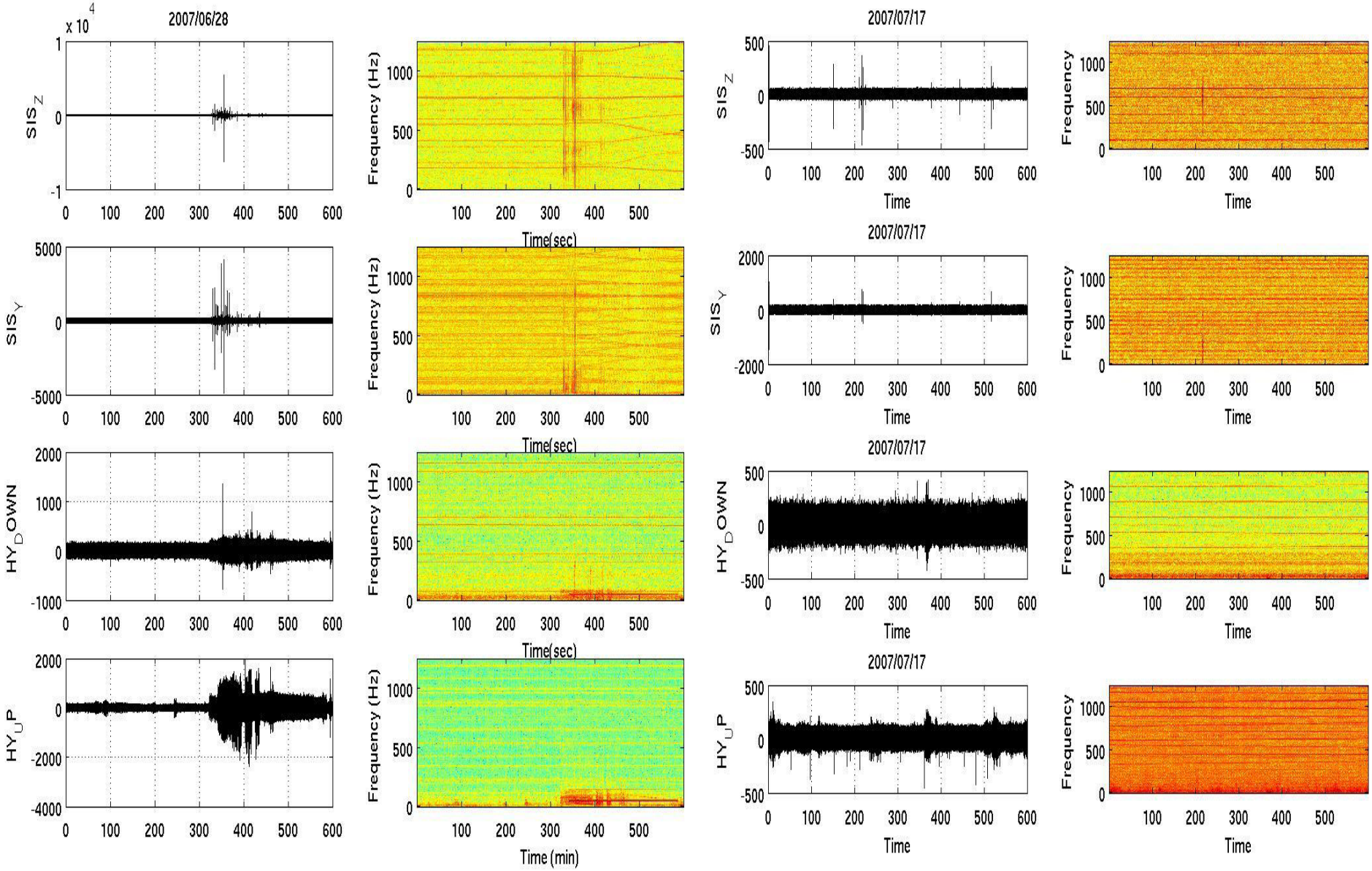
2007/06/28
x 10^4
SIS_Z
SIS_Y
HY_DOWN
HY_UP
Frequency (Hz)
Time(sec)
Time (min)
2007/07/17
Time
Frequency

Statistics for events seen on AIG10 sensors

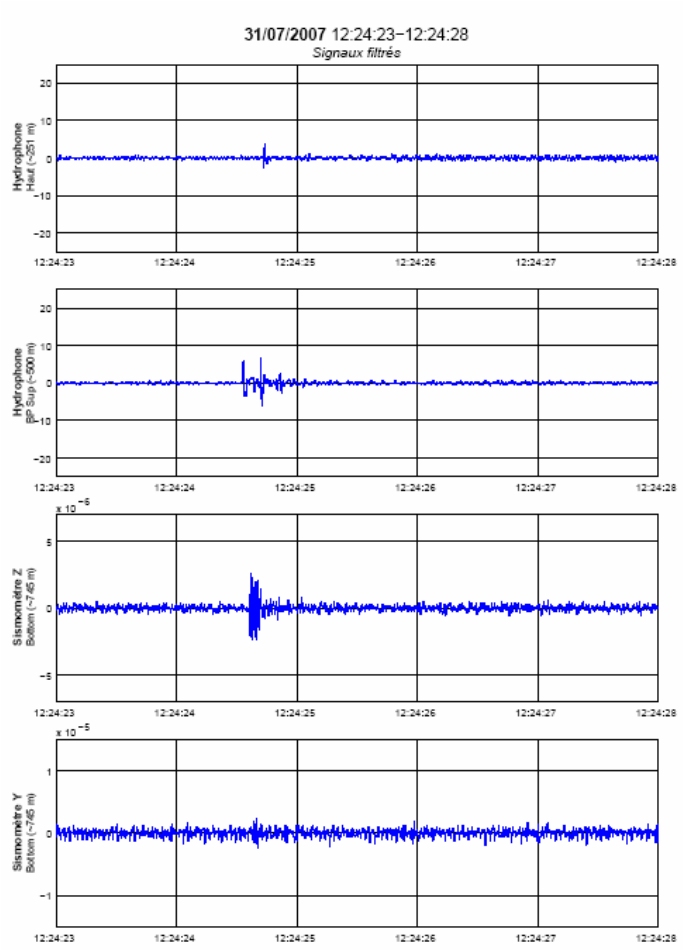

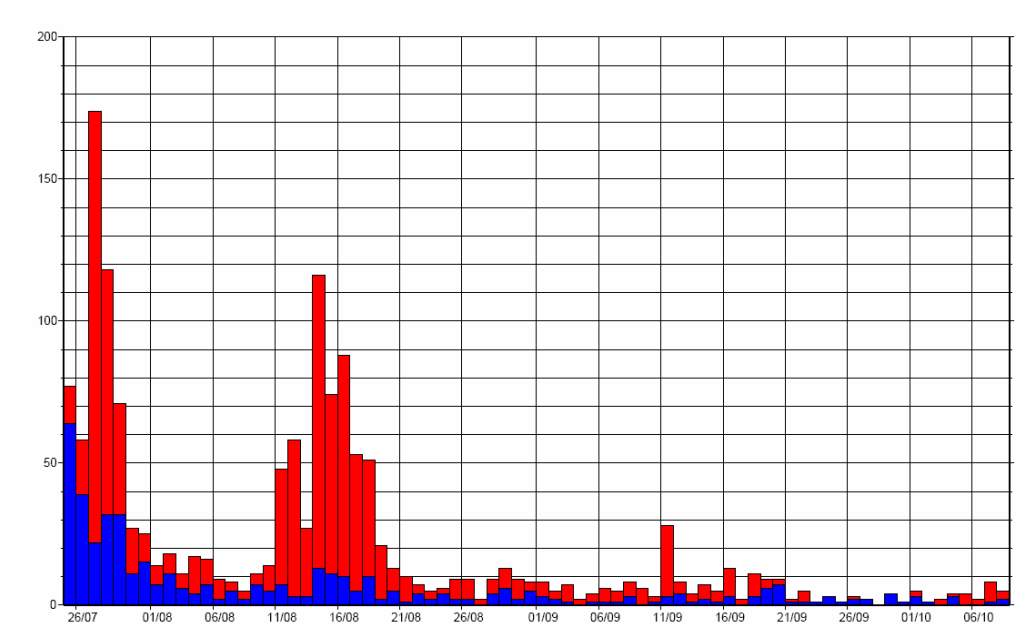

Number of events detected by AIG10 and CRLNET

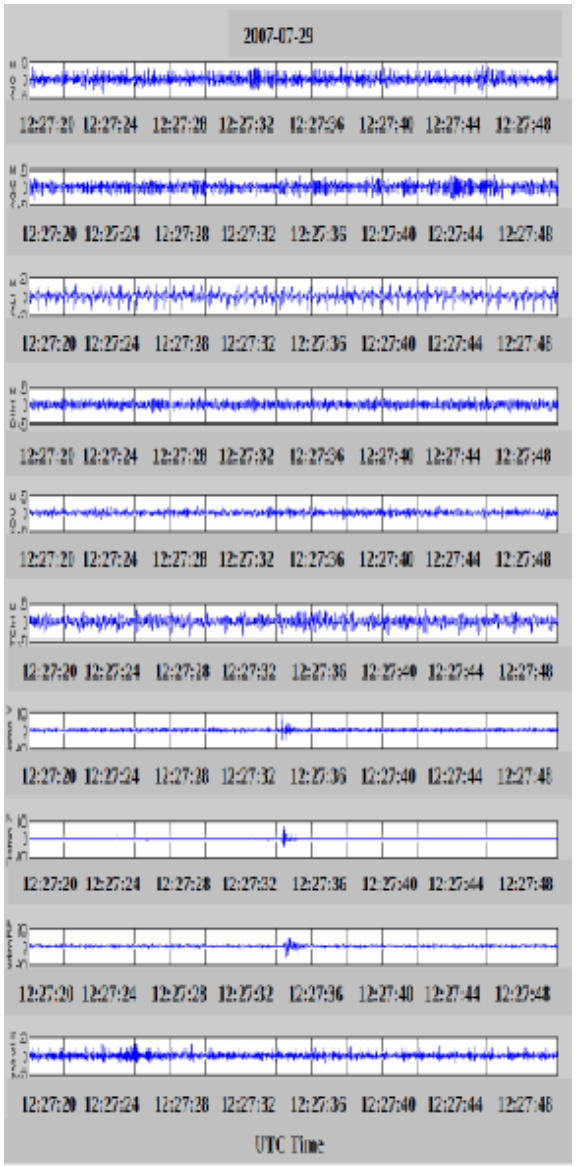

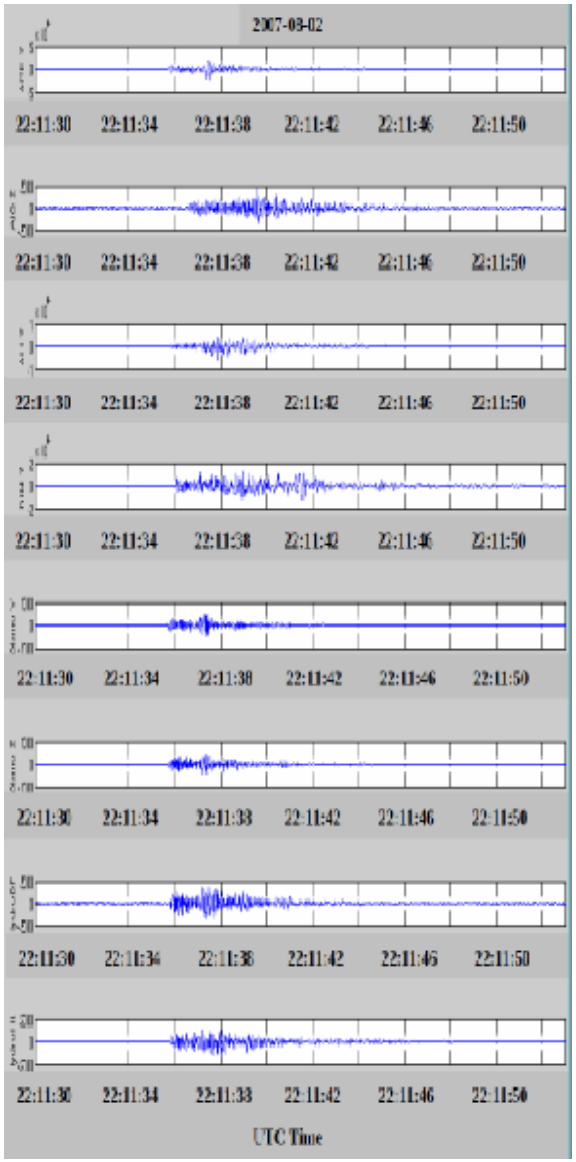

More than 1000 events are seen on the 3 stations in AIG10 and at least 3 CRLnet stations .

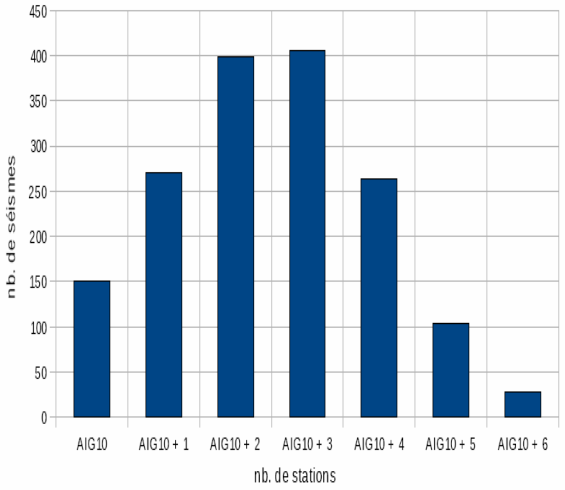

Nombre d'événements vus sur les capteurs installés dans AIG10 et un certain nombre de stations de CRLNet.

Comparison between automatic detection and location of events , as detected only with CRLnet, or with both CRLnet and AIG10 (location Hypo71)

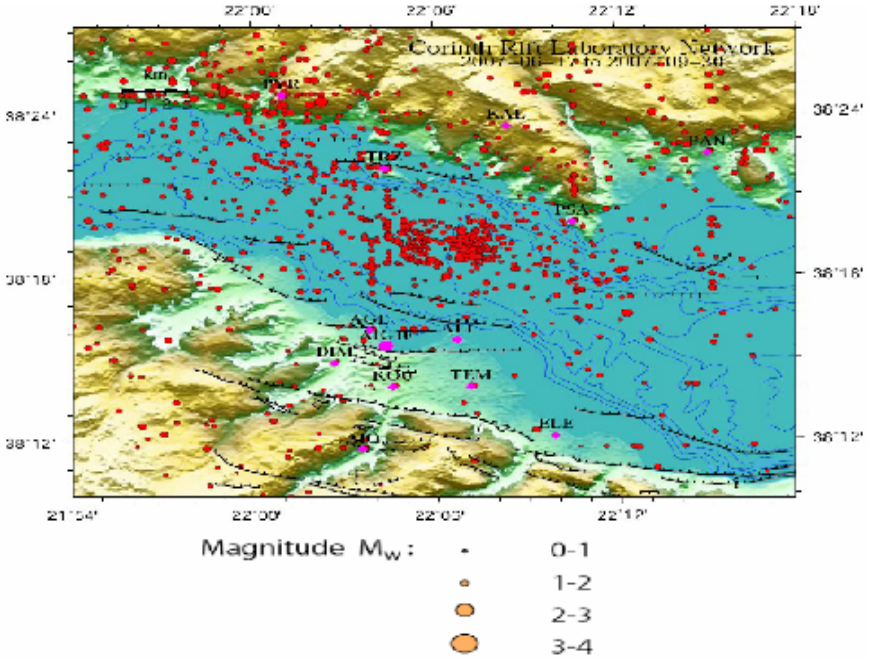

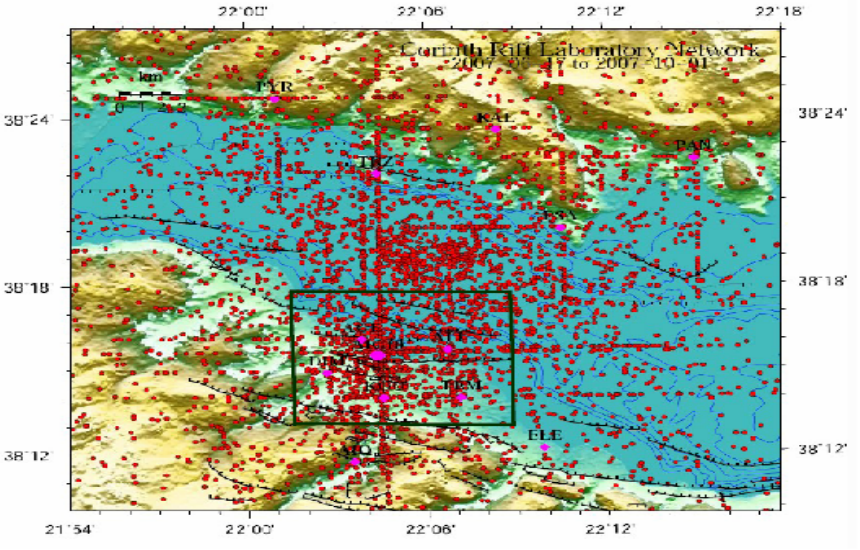

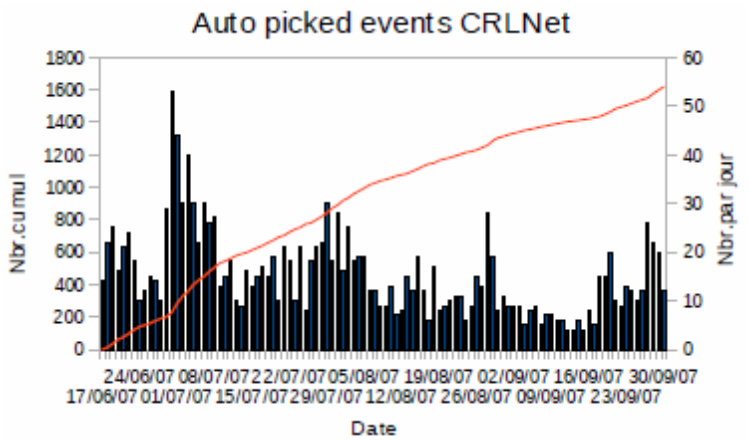

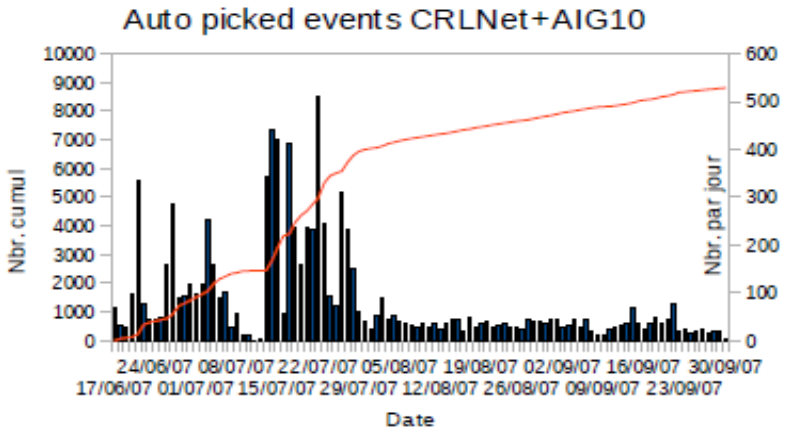

Location of events with Hypoinverse, a velocity field compatible with VSP run in AIG10 and station correction factors based on events from the rift.

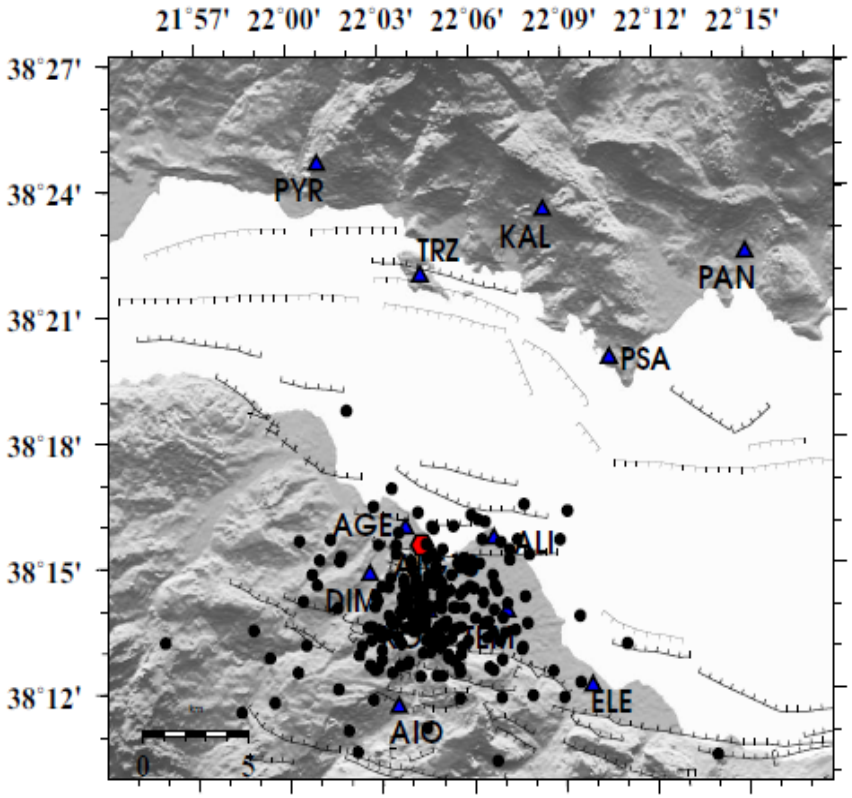

- Résidus aux stations ≤ 100 ms

P and S wave arrivals are picked manually

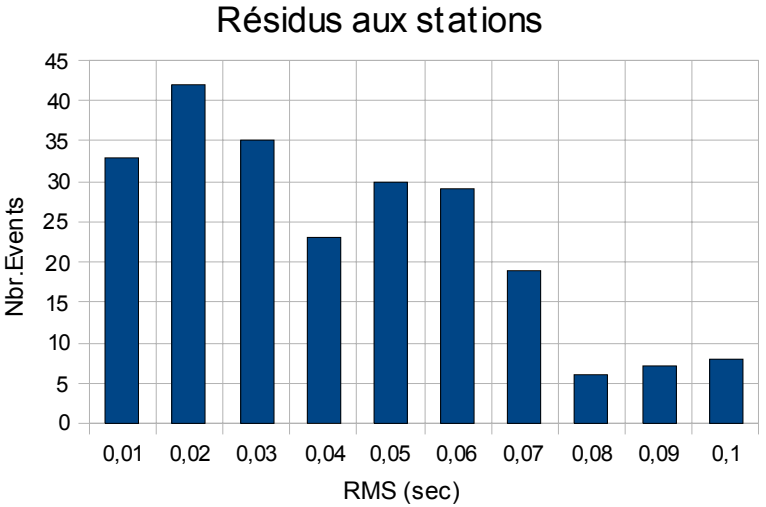

ERH ≤ 0.5 km; ERZ ≤ 0.5 km

A first analysis of the geometry of the active zone

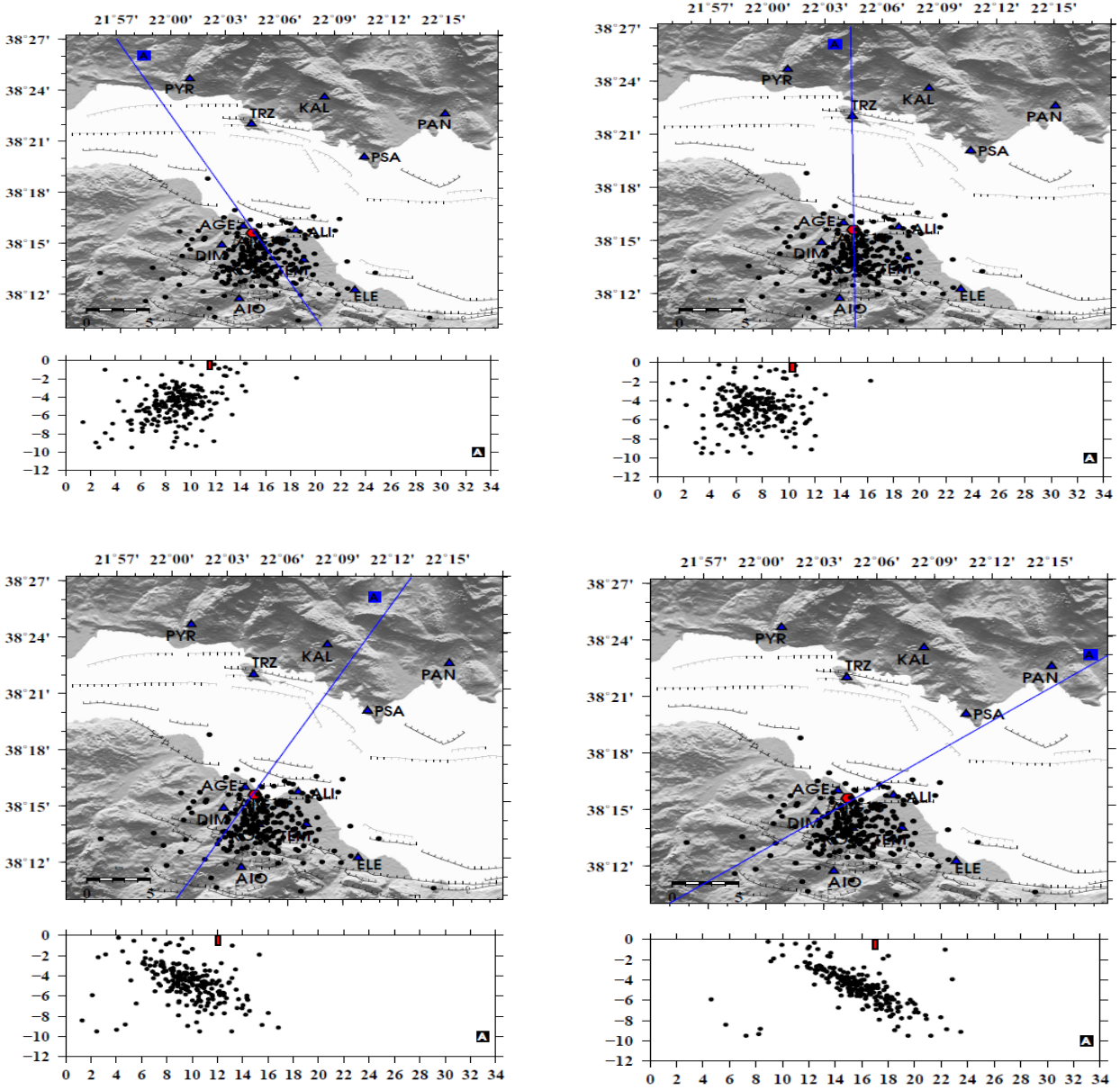

Projections in vertical planes has been run with vertical plane orientations ranging from N 90°W to N90°E, at 15° increments.

A clear planar zone oriented roughly N 30°W is identified

The planar zone may be the nappe below the Gavrovo Tripolitza. It stops at Heliki fault, and is below the AIG10 well.

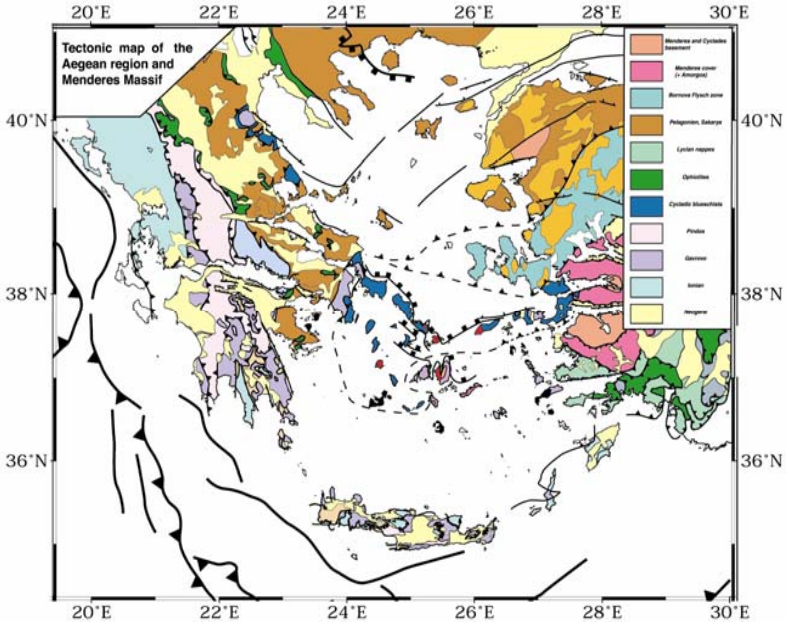

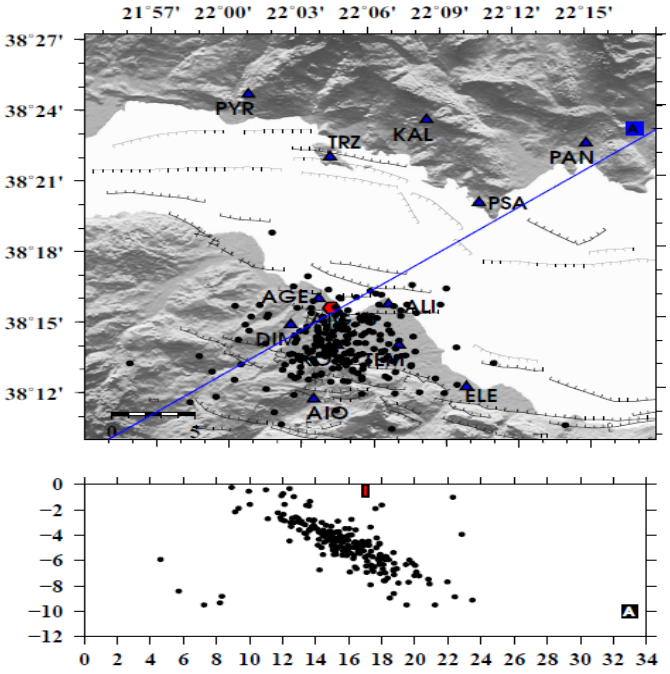

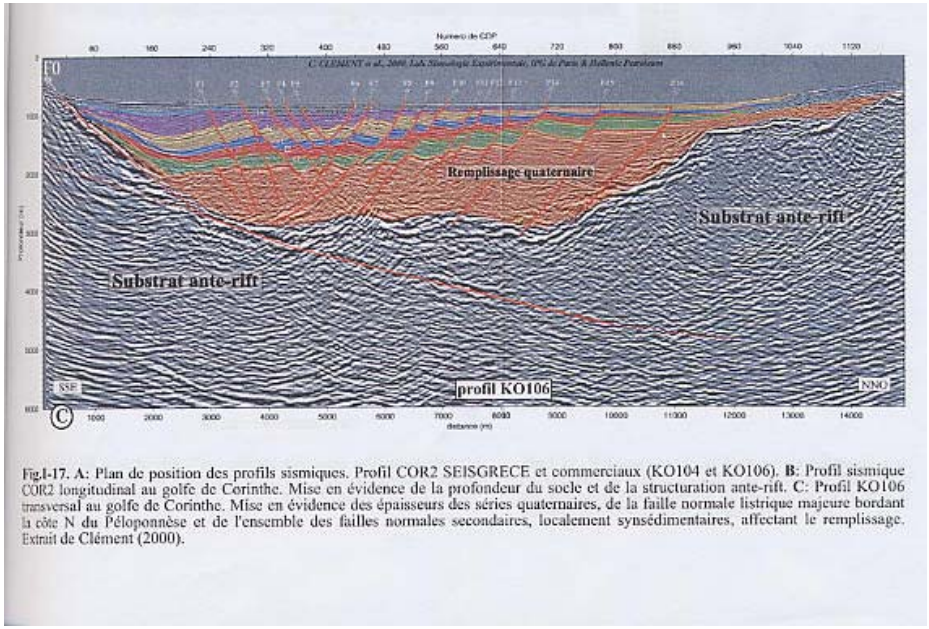

Fig.I-17. A: Plan de position des profils sismiques. Profil COR2 SEISGRECE et commerciaux (KO104 et KO106). B: Profil sismique COR2 longitudinal au golfe de Corinthe. Mise en évidence de la profondeur du socle et de la structuration ante-rift. C: Profil KO106 transversal au golfe de Corinthe. Mise en évidence des épaisseurs des séries quaternaires, de la faille normale listrique majeure bordant la côte N du Péloponnèse et de l'ensemble des failles normales secondaires, localement synsédimentaires, affectant le remplissage. Extrait de Clément (2000).

Identification of multiplets

Many multiplets are identified from AIG10 stations but the sampling rate for CRLNet stations is to slow for the frequency content of the multiplets. For these events, no multiplet is identified with CRLnet stations.

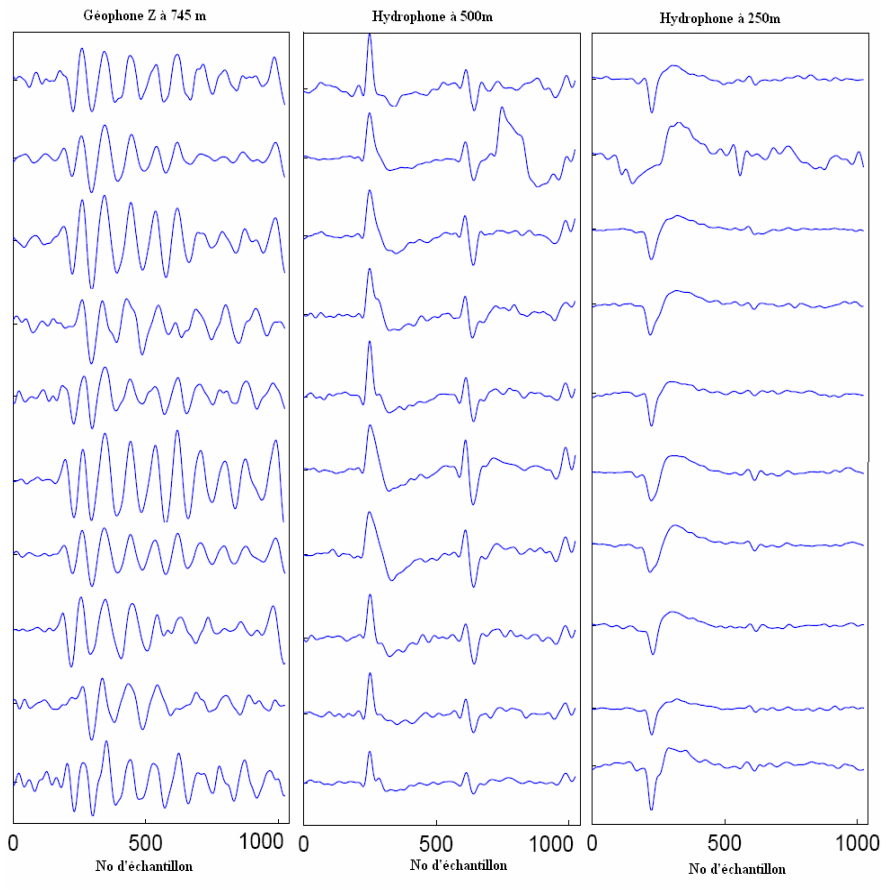

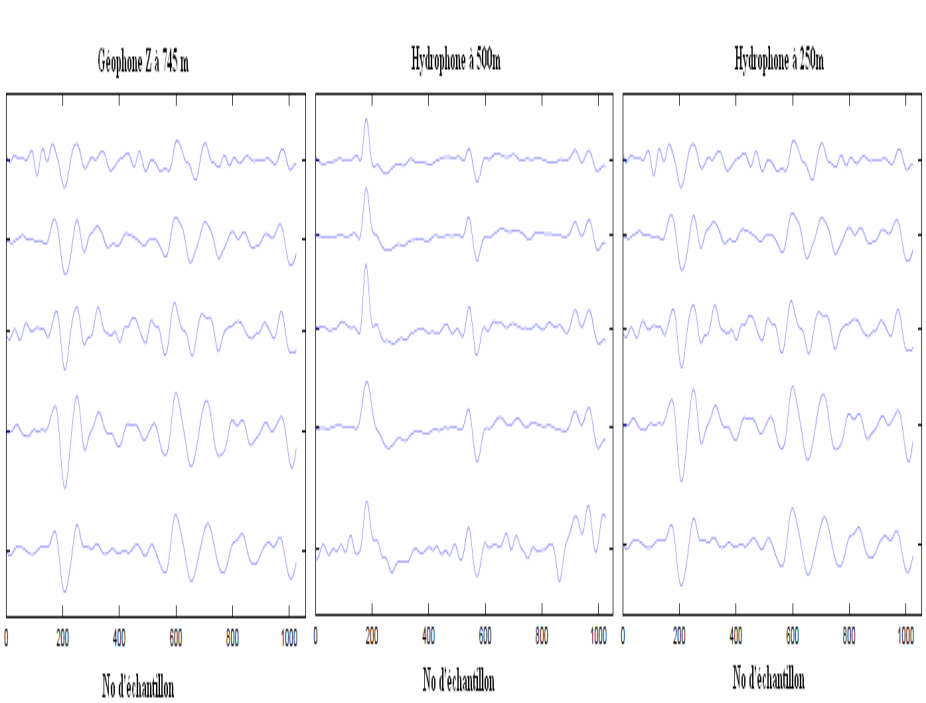

	AIG10	CRLNet
Sample frequency in Hz	: 2501	125
Maximum frequency in Hz	: 100	20
Window length	: 1024 éch	128 éch
inter-correlation level	: 0.85	0.85
Nb of stations	: 3	3

Hydro-mechanical coupling

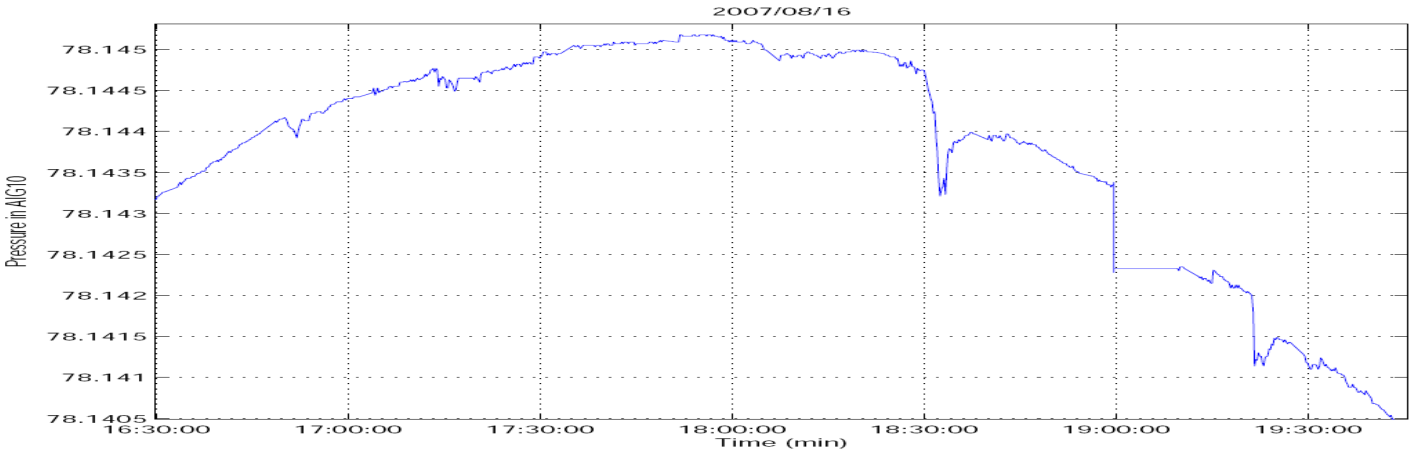

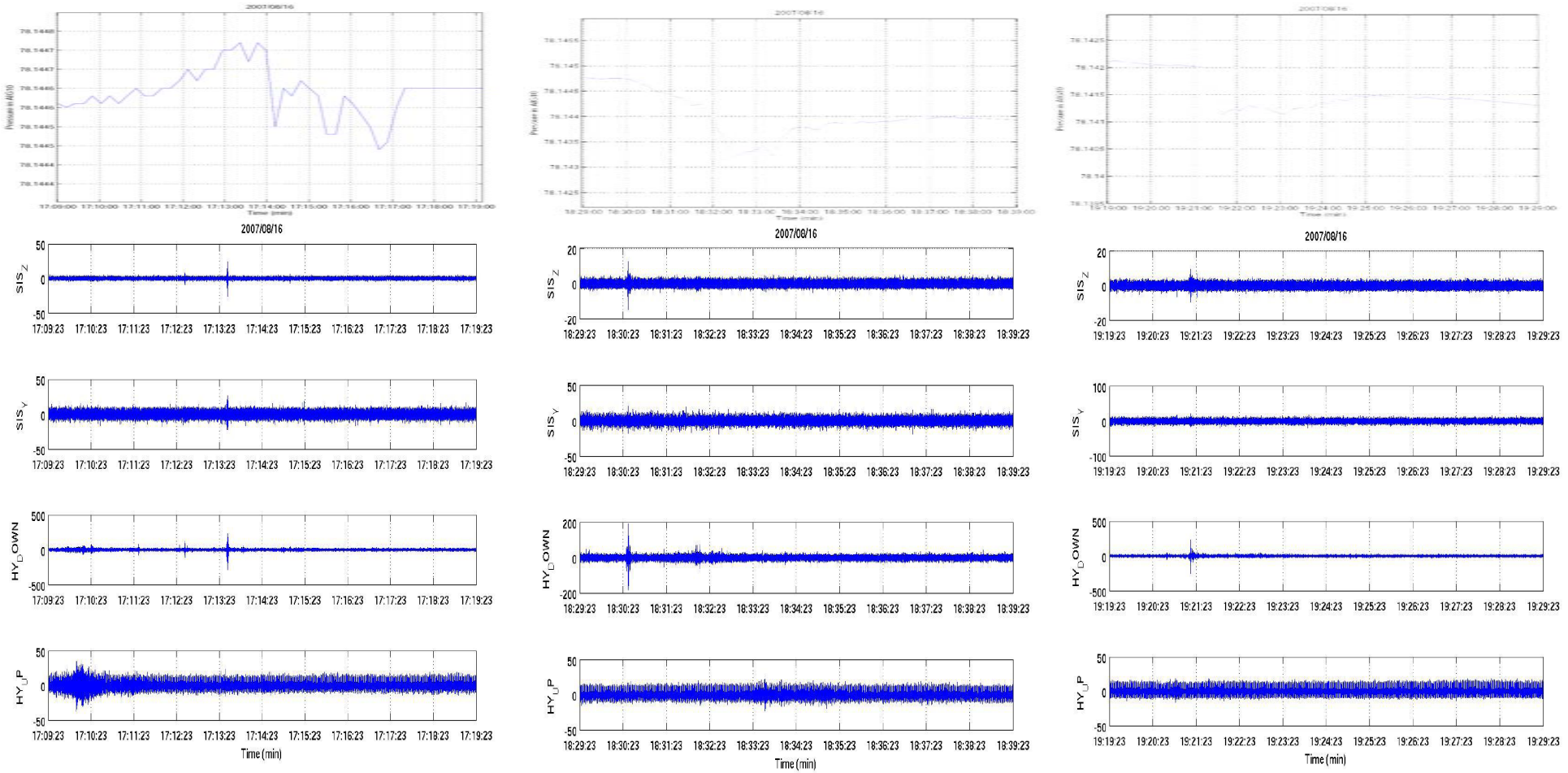

Conclusions from the Corinth Rift

- Events in the 30-1000 Hz frequency domain occur very often but go undetected with the « short period » surface network.
- They outline a creeping zone that possibly lies below the gavrovo-Triplitza nappe and may continuously unload the upper section of the steeply dipping normal faults that outcrops on the southern shore of the rift, in this region.
- This may explain the 1.5 cm horizontal rift opening, but modelling remains to be conducted.
- Comparison between pore pressure variations and observed events suggests that many creep events are associated with high frequency signals.
- A major question that remains to be addressed is whether similar observations would have been obtained had the borehole been located on the Derveni Fault, some 40 km East of Aigion, where a seismic gap is identified.

A more general conclusion

- It is generally accepted that the upper 5 km of the crust is aseismic.
- Our results demonstrate that creep may occur, but the creep events are too small to be detected individually by continuous GPS monitoring.
- High frequency sensors coupled with sensitive pore pressure monitoring may be a tool for detecting such shallow creep events and may reveal of import for earthquake prediction.
- Present tomography work at Soultz suggests they may help better understand induced seismicity observed during the development phase of Enhanced Geothermal Systems.